

# Functional Depletion of Mahogunin by Cytosolically Exposed Prion Protein Contributes to Neurodegeneration

Oishee Chakrabarti<sup>1</sup> and Ramanujan S. Hegde<sup>1,\*</sup>

<sup>1</sup>Cell Biology and Metabolism Program, National Institute of Child Health and Human Development, National Institutes of Health, Bethesda, MD 20892, USA

\*Correspondence: [hegder@mail.nih.gov](mailto:hegder@mail.nih.gov)

DOI 10.1016/j.cell.2009.03.042

## SUMMARY

The pathways leading from aberrant Prion protein (PrP) metabolism to neurodegeneration are poorly understood. Some familial PrP mutants generate increased C<sup>tm</sup>PrP, a transmembrane isoform associated with disease. In other disease situations, a potentially toxic cytosolic form (termed cyPrP) might be produced. However, the mechanisms by which C<sup>tm</sup>PrP or cyPrP cause selective neuronal dysfunction are unknown. Here, we show that both C<sup>tm</sup>PrP and cyPrP can interact with and disrupt the function of Mahogunin (Mgn), a cytosolic ubiquitin ligase whose loss causes spongiform neurodegeneration. Cultured cells and transgenic mice expressing either C<sup>tm</sup>PrP-producing mutants or cyPrP partially phenocopy Mgn depletion, displaying aberrant lysosomal morphology and loss of Mgn in selected brain regions. These effects were rescued by either Mgn overexpression, competition for PrP-binding sites, or prevention of cytosolic PrP exposure. Thus, transient or partial exposure of PrP to the cytosol leads to inappropriate Mgn sequestration that contributes to neuronal dysfunction and disease.

## INTRODUCTION

Mammalian Prion protein (PrP) is a cell-surface GPI-linked glycoprotein implicated in several neurodegenerative diseases including scrapie, bovine spongiform encephalopathy, Creutzfeldt-Jakob disease, and Gerstmann-Straussler-Scheinker disease (Aguzzi et al., 2007; Collinge and Clarke, 2007). The most extensively studied aspect of these diseases is their transmissibility via an unusual agent (termed prion) composed largely, if not exclusively, of a misfolded isoform of PrP termed PrP<sup>Sc</sup>. Prion propagation is thought to occur when PrP<sup>Sc</sup> converts the normal cellular form of PrP (PrP<sup>C</sup>) into additional copies of PrP<sup>Sc</sup>. Although this explains how altered protein conformation can form the basis of disease transmission, relatively little is known about the pathways of cellular dysfunction that culminate in neurodegeneration in PrP-associated diseases.

Because PrP<sup>Sc</sup> is highly insoluble and aggregation prone, it was long assumed that its accumulation in the central nervous system would be intrinsically harmful to neurons. However, this view appears to be overly simplistic since several experimental paradigms have partially or fully uncoupled PrP aggregate deposition from downstream neuropathology (Brandner et al., 1996; Mallucci et al., 2003; Chesebro et al., 2005). Conversely, several familial PrP mutations cause neurodegeneration with little or no generation of PrP<sup>Sc</sup> or transmissible agent (Tateishi and Kitamoto, 1995; Tateishi et al., 1996; Chiesa et al., 2003). These and other observations suggest that neurodegeneration might involve different aspects of PrP metabolism beyond just PrP<sup>Sc</sup> accumulation (Hetz and Soto, 2006; Chakrabarti et al., 2009), prompting investigation into other isoforms of PrP that might mediate neurotoxicity.

One minor isoform of PrP, termed C<sup>tm</sup>PrP, spans the membrane once (at a hydrophobic domain [HD] from residues ~112–135) with the N-terminal domain exposed to the cytosol (Hegde et al., 1998). Remarkably, both a natural and several artificial mutants within the HD that lead to even modestly increased generation of C<sup>tm</sup>PrP (between 5% and 20% of total PrP) cause neurodegeneration in transgenic mice (Hegde et al., 1998, 1999). Furthermore, several familial diseases in humans are associated with hydrophobicity-increasing mutations in the HD (e.g., A117V; Hsiao et al., 1991) that may increase C<sup>tm</sup>PrP generation (Hegde et al., 1998). Indirect evidence in transgenic mice suggests that C<sup>tm</sup>PrP levels might also be increased (or perhaps stabilized from degradation) upon PrP<sup>Sc</sup> accumulation (Hegde et al., 1999). Thus, at least a subset of familial neurodegenerative diseases, and perhaps also PrP<sup>Sc</sup>-mediated transmissible diseases, are associated with generation of C<sup>tm</sup>PrP.

In separate studies, a small proportion of PrP was found to be degraded in the cytosol by the proteasome (Yedidia et al., 2001; Ma and Lindquist, 2001). The observation that improving the efficiency of the PrP signal sequence markedly reduces the proportion of PrP degraded by the proteasome suggested that inefficient forward translocation into the ER is a major source of cyPrP (Rane et al., 2004). Interestingly, enforced cyPrP expression in transgenic mice caused neurodegeneration in a cell-type-selective manner (Ma et al., 2002). However, the relevance of this observation to either familial or transmissible disease caused by PrP has been unclear.

More recently, several observations have suggested an indirect means to potentially link cyPrP production to prion disease

pathogenesis. First, translocation of PrP into the ER is reduced during ER stress (Kang et al., 2006; Orsi et al., 2006), leading to increased cyPrP production. Second, ER stress appears to be an indirect consequence of prion infection and PrP<sup>Sc</sup> accumulation (Hetz and Soto, 2006; Rane et al., 2008). Third, reduced PrP translocation at levels comparable to that seen during ER stress was sufficient to cause mild age-dependent neurologic dysfunction in transgenic mice despite essentially quantitative degradation of cyPrP (Rane et al., 2008). And finally, proteasome activity may decline with age (Dahlmann, 2007) and upon PrP<sup>Sc</sup> accumulation (Kristiansen et al., 2007). Thus it is plausible that by the combined effects of a weak PrP signal sequence, reduced PrP translocation during ER stress, and reduced proteasome activity upon PrP<sup>Sc</sup> accumulation, cyPrP is generated in sufficient amounts during prion disease to be a contributing factor in neurodegeneration (Rane et al., 2008).

And finally, PrP<sup>Sc</sup> was shown to directly inhibit the proteasome *in vitro* (Kristiansen et al., 2007). Because proteasome activity was observed to be decreased with prion infection in cells and mice, it was proposed that cytosolic PrP<sup>Sc</sup> inhibits the proteasome to cause neuronal death during disease pathogenesis. While it is not yet clear how PrP<sup>Sc</sup> (normally formed in extracellular or endolysosomal compartments) could access the cytosol, its cytosolic mislocalization was a key point of this model. Thus, one theme that emerges from the above paradigms of neurodegeneration is the exposure of PrP to the cytosolic environment. Although only partially or very transiently exposed, this minor population of PrP could conceivably have adverse consequences for certain cells under certain conditions if it were to make inappropriate interactions with cellular factors whose functions become compromised. However, candidate interacting partners for cytosolic PrP are poorly studied and their roles in disease unknown.

In the context of this hypothesis, the cytosolic protein Mahoguin (Mgmn) is especially intriguing. Loss of Mgmn function was found to cause both the mahoganoid coat color phenotype and late-onset spongiform neurodegeneration in selected brain regions (He et al., 2003). The resemblance of Mgmn and prion disease pathology raised the possibility of a mechanistic relationship. However, a functional connection between Mgmn and PrP was not immediately apparent. Although Mgmn has E3 ubiquitin ligase activity, PrP is not a substrate *in vitro* and does not accumulate *in vivo* in the absence of Mgmn (He et al., 2003). Nevertheless, a growing appreciation that minor populations of PrP are either partially (in the case of C<sup>tm</sup>PrP) or transiently (in the case of cyPrP) exposed to the cytosol during disease led us to consider the alternative hypothesis that cytosolically mislocalized forms of PrP might interact inappropriately with Mgmn to inhibit its function. This would phenocopy Mgmn depletion, leading to region-selective neurodegeneration. Here, we examine this hypothesis using *in vitro*, cell culture, and mouse models.

## RESULTS

### Experimental Logic

Under normal circumstances, the amounts of C<sup>tm</sup>PrP and cyPrP are minor and often transient. Even mutations that favor production of these isoforms result in modest increases that, while rele-

vant for disease over long time periods in certain cell types, nonetheless make analysis of potential protein-protein interactions daunting. To circumvent this problem, we initially used artificial systems that greatly exaggerate the abundance and stability of Mgmn and cytosolically exposed PrP to explore the possibility of an interaction between them. This strategy allowed the evaluation of potential interactions, mapping of interacting domains, characterization of downstream phenotypes, and detailed functional analysis in a robust experimental system. The physiologic relevance of the results from such exaggerated systems was validated subsequently in cellular and mouse models that more accurately reflect the disease state.

### Interaction of Mgmn with Cytosolic PrP Aggregates

Expression of PrP in the cytosol leads to its rapid degradation by the ubiquitin-proteasome system. Degradation ensues regardless of whether cytosolic PrP is generated by mutation, by deletion of the signal, or by inhibitors of translocation (Ma et al., 2002; Kang et al., 2006). The very low steady-state levels of cytosolic PrP therefore make it difficult to assess a potential interaction with Mgmn *in vivo* without proteasome inhibitors that could have many indirect effects. To avoid this, we took advantage of the serendipitous observation that fluorescent protein (FP) tagged PrP lacking the N- and C-terminal signals is poorly degraded and artifactually forms aggregates in nearly all cells (Figure S1 available online). Such aggregates remained affixed in the cell upon selective release of freely diffusible cytosolic contents by digitonin-mediated semipermeabilization of the plasma membrane. We exploited these observations to develop an *in vivo* interaction assay based on coassociation of an FP-tagged test protein with FP-tagged cytosolic PrP aggregates (Figure 1A).

Coexpression of red fluorescent protein (RFP) with cyan fluorescent protein (CFP)-PrP<sub>40-231</sub> (CFP fused to residues 40–231 of PrP) followed by digitonin permeabilization led to a rapid and essentially complete loss of RFP signal (within ~2–5 min) from the nucleocytoplasmic compartment (Figures 1B and S1). By contrast, RFP-Mgmn was partially retained in the cell upon permeabilization, colocalizing precisely with aggregates formed by CFP-PrP<sub>40-231</sub> (Figures 1C and S1). Coaggregation was seen with PrP and Mgmn regardless of the FP tags used (we have used CFP, green fluorescent protein [GFP], and RFP in various combinations), in cells with widely varying expression levels of Mgmn (spanning at least 20-fold), and with aggregates of various sizes and morphology (unpublished data). Evidence for an interaction between RFP-Mgmn and CFP-PrP<sub>40-231</sub> could also be observed without permeabilization, especially in cells where the RFP-Mgmn was expressed at lower levels and the nonaggregated population did not confound the imaging (Figures 1C and S1). Furthermore, the observation that RFP-Mgmn was typically retained in coassociation with the aggregate over an hour after permeabilization (unpublished data) suggests that its sequestration was not rapidly reversible. Importantly, Mgmn sequestration was specific to PrP aggregates since aggregates formed by a GFP-tagged Huntingtin (Htt) fragment containing 103 glutamines failed to coassociate with RFP-Mgmn (Figure 1D). Thus, mislocalized PrP (artificially immobilized into aggregates in this case) can interact selectively with Mgmn in cultured cells.

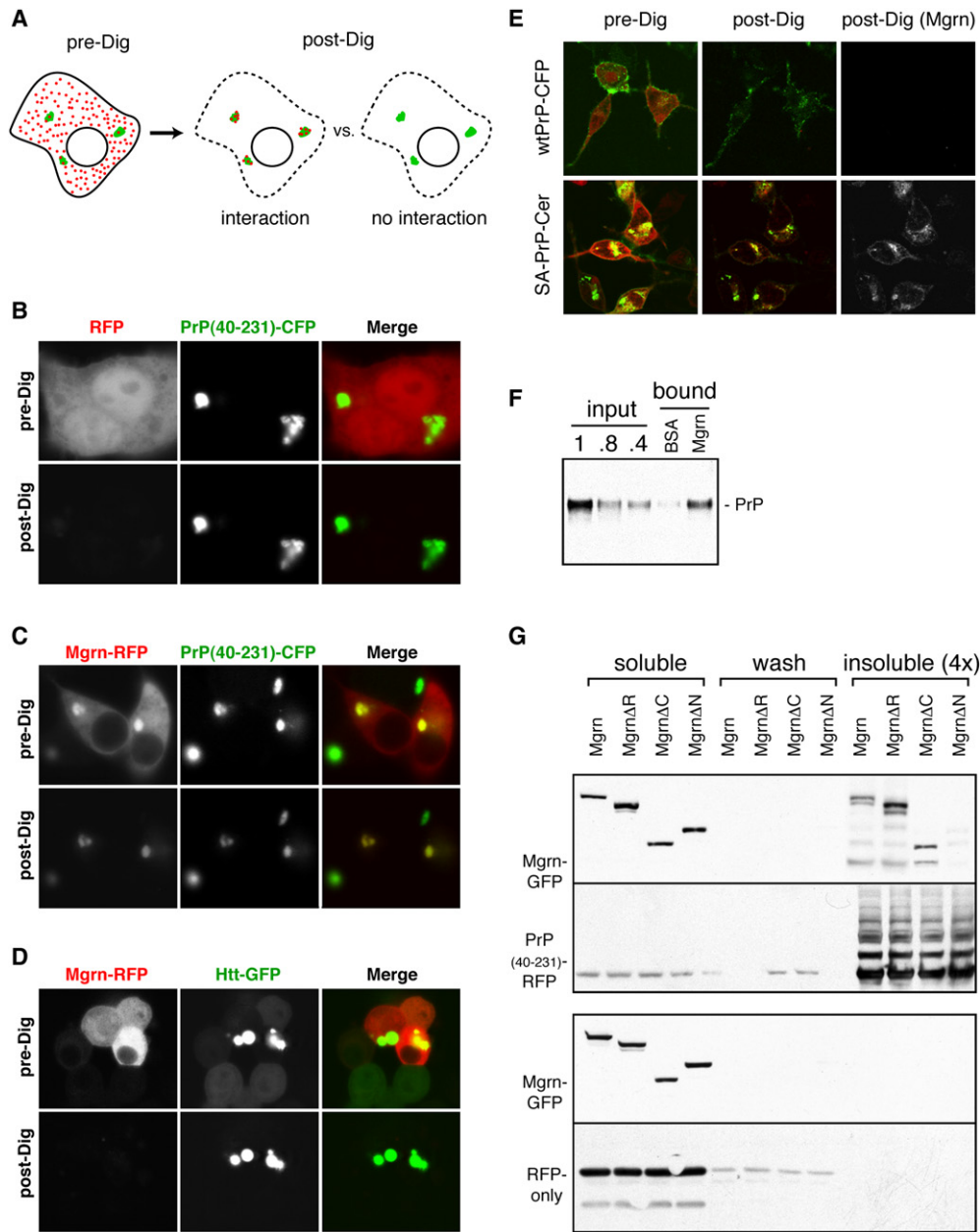


**Figure 1. Mahogunin Interacts with Cytosolically Exposed PrP**

(A) Experimental design to detect a potential interaction between two proteins (red and green), one of which remains immobilized upon semipermeabilization of the plasma membrane with digitonin.

(B–D) N2a cells cotransfected with the indicated FP-tagged constructs were imaged before (“pre-Dig”) or after (“post-Dig”) digitonin semipermeabilization for 10 min. Note that RFP-Mgrn is partially retained with aggregates of CFP-PrP<sub>40–231</sub>, but not Htt-GFP, after permeabilization.

(E) RFP-Mgrn (red) was transfected into cells stably expressing SA-PrP-Cer or PrP-CFP (green) and analyzed by the digitonin coassociation assay as in (B). Images before and after permeabilization are shown. RFP-Mgrn is partially retained by SA-PrP-Cer, but not PrP-CFP.

(F) A detergent lysate of normal adult hamster was passed over columns of immobilized BSA or Mgrn, and the bound products (along with different amounts of input brain lysate) were analyzed by immunoblot for PrP.

(G) RFP-PrP<sub>40–231</sub> (top panels) or RFP (bottom panels) was coexpressed in N2a cells with the GFP-Mgrn constructs indicated above each lane. The cells were fractionated into a cytosolic (soluble) fraction, Triton X-100 wash fraction, and insoluble fraction (4-fold more loaded relative to the other fractions) and immunoblotted with anti-GFP (to detect the Mgrn constructs) and anti-RFP (to detect RFP-PrP<sub>40–231</sub> aggregates or RFP).

### Interaction of Mgrn with Transmembrane PrP

We applied the same semipermeabilization assay to also illustrate an interaction between Mgrn and  $C^{tm}$ PrP. We first generated and characterized cell lines expressing FP-tagged wild-type PrP or SA-PrP, a construct made exclusively in the  $C^{tm}$ PrP form (Figure S2). RFP-Mgrn expressed in these cells was then analyzed before and after digitonin semipermeabilization. While RFP-Mgrn was fully extracted from cells expressing wild-type PrP, it was significantly retained in the SA-PrP cells (Figure 1E). The retained RFP-Mgrn decorated the plasma membrane and intracellular membranous structures containing SA-PrP. Thus, PrP forced into the  $C^{tm}$ PrP topology permits an interaction with Mgrn, whereas wild-type PrP does not (presumably a consequence of its lack of exposure to the cytosol).

### Biochemical Validation of PrP-Mgrn Interactions

The key interactions observed between Mgrn and PrP could also be demonstrated biochemically in two ways. In the first experiment, PrP from a detergent-solubilized crude brain lysate could be pulled down more efficiently by immobilized recombinant Mgrn than the immobilized BSA control (Figure 1F). In the second experiment, we coexpressed RFP-PrP aggregates with different GFP-Mgrn constructs lacking the N terminus, C terminus, or RING domain. The cells were then separated into soluble cytosol, wash, and insoluble fractions. Immunoblotting revealed that essentially all of the RFP-PrP was found in the insoluble fraction, consistent with its predominantly aggregated status seen visually (Figure 1G). Significant GFP-Mgrn, -Mgrn $\Delta$ C, and -Mgrn $\Delta$ R were also recovered with the insoluble fraction, while noticeably less GFP-Mgrn $\Delta$ N was recovered (Figure 1G, top panel). Importantly, none of the Mgrn constructs were seen in the insoluble fraction in cells lacking PrP aggregates (Figure 1G, bottom panel). Thus, cytosolically exposed PrP can interact with Mgrn (via its N terminus; see next section). This interaction is not normally seen with wild-type PrP (even though it is *capable* of interacting; Figure 1F), presumably because the two proteins are in distinct compartments separated by a membrane barrier.

### Mapping the Interaction Domains of Mgrn and PrP

Serial truncations of the cytosolic GFP-PrP construct (all of which formed cytosolic aggregates; Figure S3) combined with the digitonin coaggregation assay allowed us to map the key region of PrP interacting with Mgrn (Figure 2A). Interaction was abruptly lost upon deletion from residues 84 to 95, when the last of four identical octapeptide repeats (ORs) is removed from the construct. An immobilized synthetic peptide encoding the OR sequence (PHGGGWGQ) could pull-down Mgrn, but not Mgrn $\Delta$ N or GFP, from the cytosol of cells coexpressing these proteins (Figure 2B). Neither Mgrn nor FP-Mgrn were captured by control beads lacking peptide (Figure 2C) or beads conjugated with irrelevant proteins (such as Protein A or Concanavalin A; data not shown). Deletion constructs of Mgrn showed that the N terminus, in particular the region between residues 199 and 251, was involved in the interaction with cytosolic PrP aggregates (Figures 2A, S4A, and 1G). Importantly, Mgrn need not be functional for this interaction since a construct lacking the RING domain (termed Mgrn $\Delta$ R) still interacts with PrP. Appending only residues 200–250 of Mgrn to an FP was sufficient to

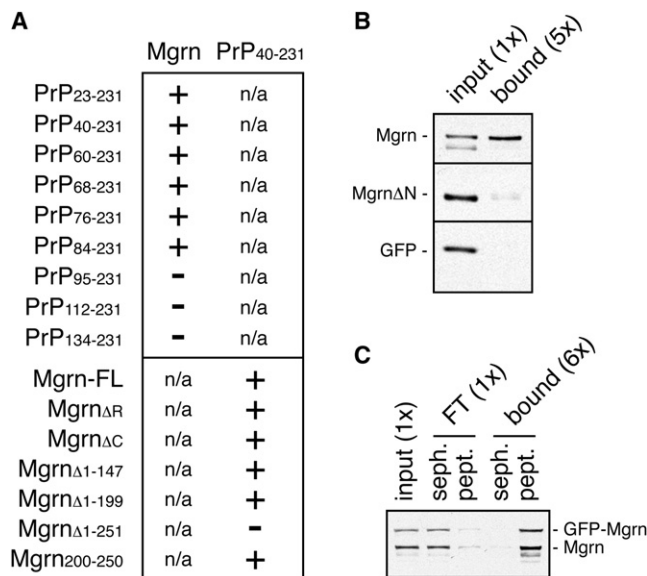


### Figure 2. Mapping the Interaction Domains in PrP and Mgrn

(A) Deletion constructs of FP-tagged PrP and Mgrn were assayed for interaction as in Figure 1.

(B) Cytosol from cells coexpressing Mgrn, Mgrn $\Delta$ N, and GFP were incubated with octapeptide-conjugated beads. Aliquots of the input and bound (5-fold excess) fractions were analyzed by immunoblotting with anti-Mgrn and anti-GFP.

(C) Cytosol from cells coexpressing Mgrn and GFP-Mgrn were incubated with sepharose beads ("seph.") or beads conjugated with the PrP octapeptide ("pept."). Aliquots of the input, unbound, and bound (6-fold excess) fractions were analyzed by immunoblotting with anti-Mgrn antibody.

allow interaction with cytosolic PrP aggregates (Figure S4B). Thus, this 50 residue domain within the N-terminal half of Mgrn interacts with the 8 residue OR sequence, four of which are present in the N-terminal half of PrP.

### Cytosolic PrP Aggregates Lead to Altered Lysosomal Morphology

The observation that overexpressed FP-Mgrn can interact with cytosolically exposed PrP raised the possibility that PrP could similarly sequester endogenous Mgrn to affect its function. Although the functional role or physiologic substrates of Mgrn are not known, its depletion by siRNA was shown to affect lysosomal morphology (Kim et al., 2007; see Figure 3B). We therefore used altered lysosome morphology as a phenotypic readout of functional Mgrn depletion to ask whether cytosolically exposed PrP would sufficiently influence endogenous Mgrn localization to at least partially phenocopy a Mgrn depletion.

Antibodies selective to Mgrn (Figure S5A) revealed that unlike overexpressed Mgrn, endogenous Mgrn is localized in widely distributed puncta (Figure S5B) that partially colocalize with markers of the endolysosomal system (Kim et al., 2007; data not shown). Upon cytosolic GFP-PrP<sub>40-231</sub> expression, Mgrn localization was altered, with clear cosequestration of at least some Mgrn around the most prominent PrP aggregates (Figure 3A). It should also be noted that the redistributed Mgrn that is not with the PrP aggregate also seems to colocalize

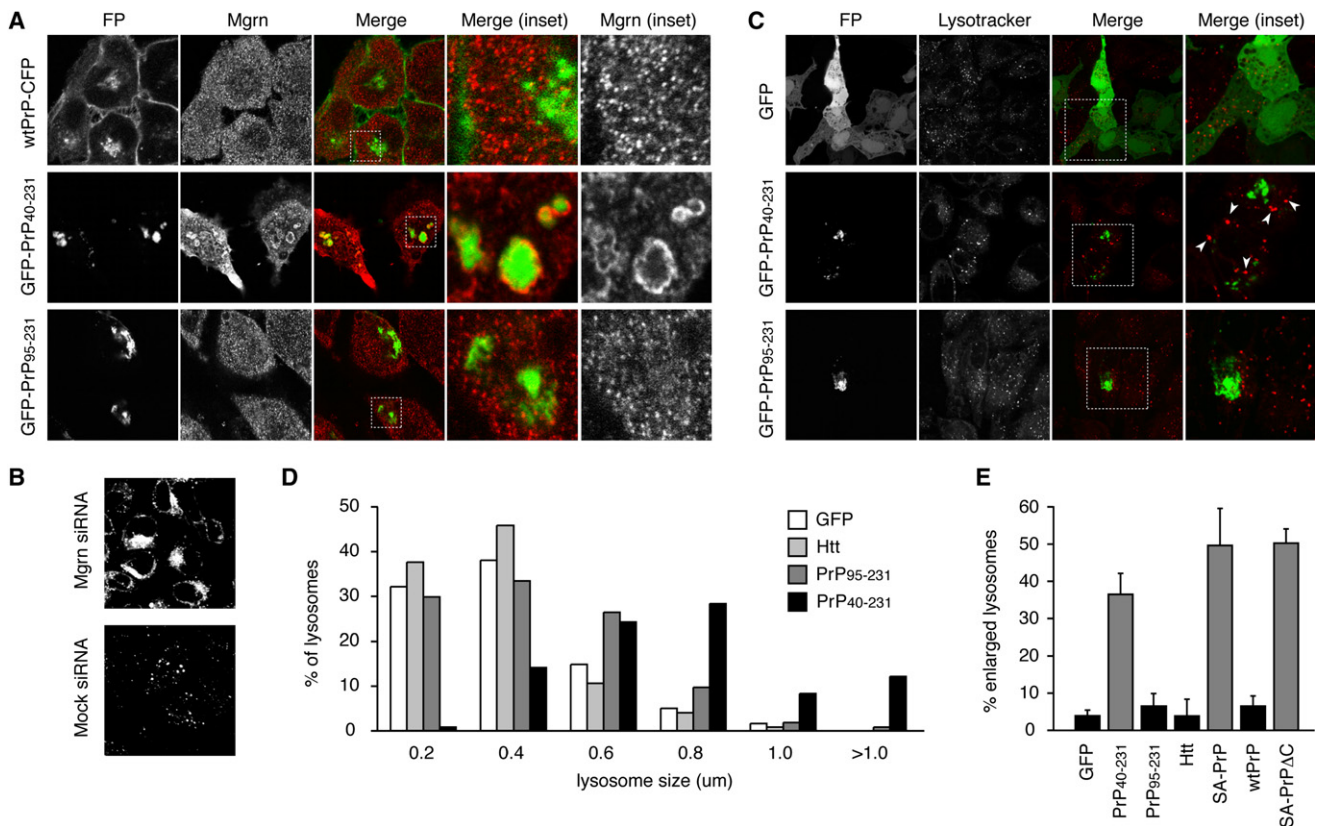


### Figure 3. Sequestration of Mgrn by Cytosolically Exposed PrP Phenocopies Mgrn Depletion

(A) HeLa cells transfected with the indicated FP-tagged PrP constructs were analyzed by indirect immunofluorescence for endogenous Mgrn. Enlarged views of the areas within the white boxes (insets) are also shown. Note that the normally punctate pattern of Mgrn expression (as in the presence of wild-type [wt]PrP-CFP and GFP-PrP<sub>95-231</sub>) was disrupted in GFP-PrP<sub>40-231</sub> expressing cells, where Mgrn is partially sequestered around the aggregates.

(B) HeLa cells transfected with Mgrn siRNAs or irrelevant siRNAs were stained with LysoTracker. Mgrn knockdown causes lysosomal enlargement and clustering. (C) HeLa cells transfected with GFP, GFP-PrP<sub>40-231</sub>, or GFP-PrP<sub>95-231</sub> were stained to visualize lysosomes as in (B). Enlarged views reveal several larger lysosomal structures in GFP-PrP<sub>40-231</sub> expressing cells (arrowheads).

(D) Histogram plotting the percentage of total lysosomes (y axis) at each of the sizes indicated on the x axis. Over 120 lysosomal structures from at least 25 cells are represented for each condition.

(E) HeLa cells transfected with the indicated constructs were analyzed for lysosomal morphology as in (D). The percent of lysosomal structures that are enlarged (defined as greater than 0.8 μm) is plotted (mean ± standard deviation [SD]). Grey bars indicate PrP constructs that interact with Mgrn.

with PrP that is not visible at this detector gain but either is found in dimmer aggregates or is diffusely cytosolic (unpublished data). This redistribution was specific to cytosolic PrP aggregates, given that wild-type PrP, Htt aggregates, and GFP-PrP<sub>95-231</sub> aggregates (lacking the octapeptide repeat domains) caused no noticeable changes in Mgrn localization (Figure 3A and data not shown). Because endogenous Mgrn appears to normally be associated tightly with membranes, we could not use selective digitonin extraction to biochemically separate PrP aggregate-associated Mgrn from normal Mgrn. That notwithstanding, the striking correlation between altered endogenous Mgrn localization and PrP constructs that in independent experiments interact with overexpressed FP-Mgrn (e.g., Figures 1 and 2) argues strongly for a physical sequestration and/or redistribution by cytosolically exposed PrP.

To assess whether this redistribution might affect Mgrn function, the lysosomal morphology and distribution in these cells were visualized with LysoTracker. A change in lysosomal appear-

ance toward larger structures (either larger lysosomes, or possibly clustering) was noted in cells expressing GFP-PrP<sub>40-231</sub> aggregates, but not GFP, GFP-Htt aggregates, or GFP-PrP<sub>95-231</sub> (Figure 3C and data not shown). A histogram of the diameters of lysoTracker-stained structures (Figure 3D) showed a clear shift in size: while only ~5%–10% of lysosomal structures were 0.8 μm or larger in control cells, such enlarged structures represented up to ~50% of staining particles in GFP-PrP<sub>40-231</sub> aggregate-containing cells. Importantly, the distribution of lysosomal sizes in both Htt and GFP-PrP<sub>95-231</sub> aggregate-containing cells was similar to that in control cells, with less than 10% of lysosomes greater than 0.8 μm (Figure 3D). Using this diameter as a cutoff for assessment of “enlarged” lysosomes, we could quantitatively compare morphologic effects upon expression of different PrP or Mgrn constructs. Because lysosomes were quantified individually, this assay has the capacity to discern partial effects (e.g., only some of the cell’s lysosomes being enlarged) that might be expected from partial Mgrn depletion.

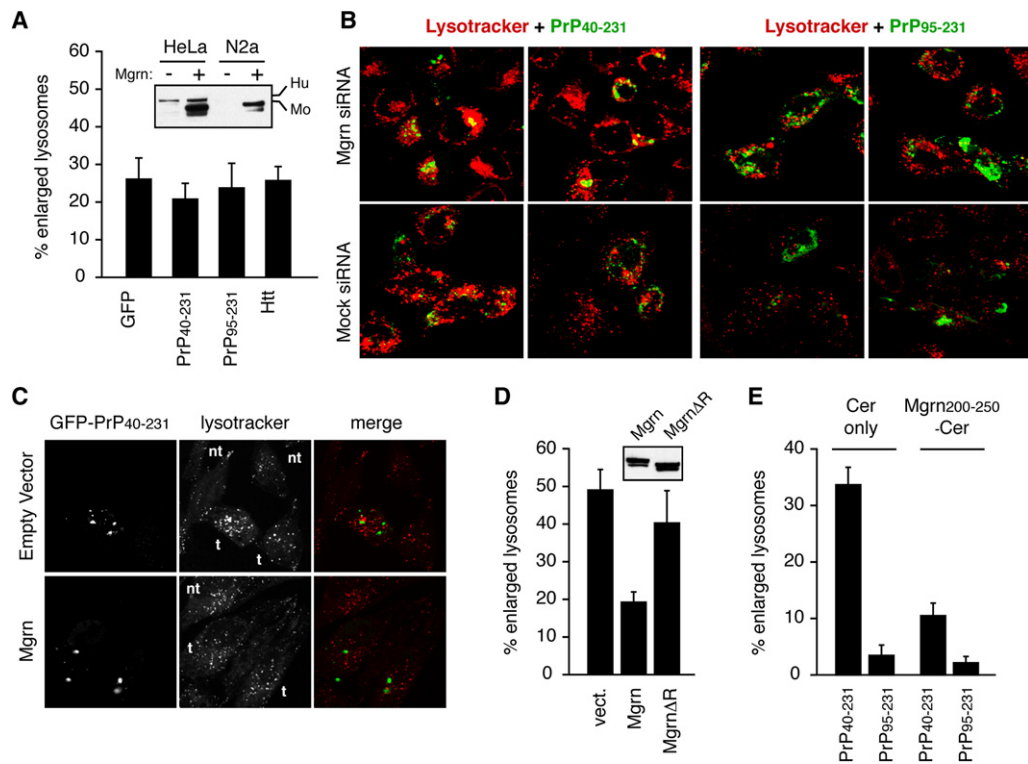


**Figure 4. Lysosomal Morphology Defect Caused by PrP Is Mediated via Mgrn**

(A) The effect of several constructs on lysosomal morphology was analyzed in N2a cells and plotted (mean  $\pm$  SD). The inset shows an anti-Mgrn immunoblot of HeLa and N2a cells that had or had not been transfected with mouse Mgrn (which serves as a positive control). Mgrn was not detectable in N2a cells. Note that human Mgrn is slightly larger than mouse Mgrn.

(B) HeLa cells treated with Mgrn siRNAs (upper panels) or irrelevant siRNAs (lower panels) were transfected with GFP-PrP<sub>40-231</sub> (left panels) or GFP-PrP<sub>95-231</sub> (right panels) and stained with Lysotracker. Two fields for each condition are shown. Note that GFP-PrP<sub>40-231</sub> closely phenocopies Mgrn knockdown, and no additional effect is seen when these two treatments are combined.

(C) HeLa cells cotransfected with GFP-PrP<sub>40-231</sub> and either empty vector or Mgrn were stained with Lysotracker. The enlarged lysosomal morphology caused by PrP aggregates was reverted by coexpression of Mgrn (quantified in D). Transfected (t) and nontransfected (nt) cells are indicated for comparison.

(D) GFP-PrP<sub>40-231</sub> was cotransfected with either empty vector, Mgrn, or the catalytically inactive Mgrn $\Delta$ R and analyzed for lysosomal morphology in HeLa cells (mean  $\pm$  SD). Note that while coexpressing Mgrn rescued the disrupted lysosomal morphology to near wild-type levels, Mgrn $\Delta$ R did not. Inset shows comparable expression levels of Mgrn and Mgrn $\Delta$ R in these cells.

(E) GFP-PrP<sub>40-231</sub> or GFP-PrP<sub>95-231</sub> were cotransfected with Cerulean (Cer; a variant of CFP) or Mgrn<sub>200-250</sub>-Cer and analyzed for lysosomal morphology in HeLa cells (mean  $\pm$  SD). Note that Mgrn<sub>200-250</sub>-Cer rescues the enlarged lysosomal phenotype, presumably by shielding Mgrn-binding sites on GFP-PrP<sub>40-231</sub> (see Figure S4B).

### The Lysosomal Phenotype Caused by cyPrP Aggregates Results from Mgrn Depletion

The specificity of the lysosomal phenotype to Mgrn depletion (and not other effects of cytosolic aggregates) was validated in five ways. First, we could show that the change in lysosomal morphology correlated precisely with constructs that were shown in earlier experiments to interact with Mgrn and cause its redistribution (Figure 3E). Second, we observed that in a cell type that does not express any endogenous Mgrn (the commonly used N2a cell line), no changes in lysosomal morphology were seen upon expression of the same PrP constructs that otherwise have dramatic effects on lysosomes in HeLa cells (Figure 4A). Third, the most severe phenotypes seen in cells containing GFP-PrP<sub>40-231</sub> aggregates closely mirrored that seen with siRNA knockdown of Mgrn, and the two treatments were not further additive (Figure 4B). Fourth, the lysosomal morphology phenotype could be partially reverted by overexpression of functional Mgrn, but not a catalytically inactive Mgrn lacking the RING

domain (Figures 4C and 4D). And fifth, overexpression of Mgrn<sub>200-250</sub> tagged with Cerulean (Cer; a variant of CFP), which interacts with PrP (Figure S4B) and can therefore compete for endogenous Mgrn, substantially rescued the lysosomal phenotype (Figure 4E). Note that this competition also explains the subtle (but reproducible) partial rescue seen with Mgrn $\Delta$ R (Figure 4D), which typically expresses at more modest levels than Mgrn<sub>200-250</sub>-Cer. Considered together, these results show that cytosolically exposed PrP, whether presented as aggregates or as a transmembrane protein in the C<sup>tm</sup>PrP topology, interacts with Mgrn, influences its localization, and at least partially phenocopies Mgrn depletion to cause lysosomal morphology changes.

### Relevance of PrP-Mgrn Interaction to Disease-Causing PrP Mutants

While SA-PrP and GFP-PrP<sub>40-231</sub> are quantitatively exposed to the cytosol (in either the C<sup>tm</sup>PrP topology or as aggregates), only a small proportion of total PrP is likely to become exposed

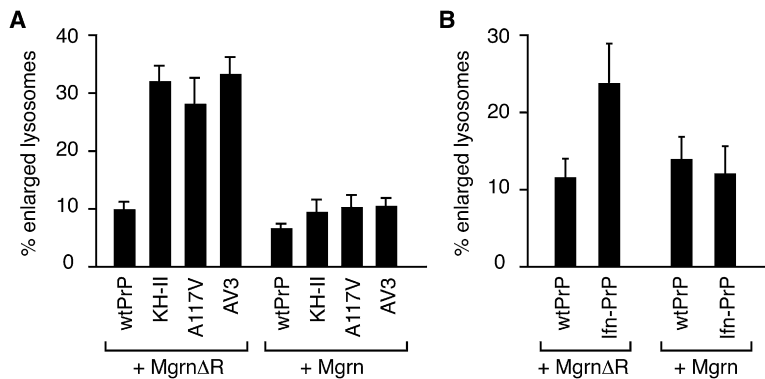


**Figure 5. Disease-Associated PrPs Lead to Aberrant Lysosomes in a Mgrn-Dependent Manner**

(A) HeLa cells transfected with the indicated PrP constructs and either functional or inactive (MgrnΔR) Mgrn were analyzed for lysosomal morphology. The percent of enlarged lysosomes is plotted (mean ± SD).

(B) The indicated PrP constructs were analyzed as in (A), except that cells were treated with proteasome inhibitor (10 μM MG132) for 4 hr immediately prior to analysis. The percent of enlarged lysosomes is plotted (mean ± SD). Note that while proteasomal inhibition marginally affects the lysosomal size for wild-type PrP (wtPrP) cells, there is an increase in the % of enlarged lysosomes in lfn-PrP cells that is reverted by Mgrn, but not MgrnΔR.

to the cytosol during either inherited or transmissible diseases caused by PrP. To assess whether situations of only partial PrP exposure would also have similar effects, we analyzed several <sup>C<sup>tm</sup></sup>PrP-favoring mutants previously characterized in transgenic mouse models (Hegde et al., 1998, 1999). These included the artificial mutants PrP(AV3) and PrP(KH-II), as well as the naturally occurring human disease mutation PrP(A117V). These constructs were coexpressed with either wild-type Mgrn or the catalytically inactive MgrnΔR, and the lysosomal morphology was assessed by quantitative microscopy (Figure 5A). Little or no change in lysosomal morphology was noted in Mgrn- or MgrnΔR-expressing cells with wild-type PrP, consistent with the fact that wild-type PrP does not substantially interact with Mgrn. By contrast, each of the <sup>C<sup>tm</sup></sup>PrP-favoring mutants showed increased proportions of enlarged lysosomes in the catalytically inert MgrnΔR-expressing cells. Importantly, coexpressing these same constructs with Mgrn reverted the lysosomal morphology close to wild-type levels. It should be further noted that these mutants showed a less dramatic effect on lysosomal morphology (as judged by % enlarged lysosomes) compared to SA-PrP, consistent with the fact that they only partially generate <sup>C<sup>tm</sup></sup>PrP.

In another experiment, we asked whether cytosolic PrP generated as a consequence of reduced PrP translocation could affect lysosomal morphology in a Mgrn-dependent manner. For this purpose, we used lfn-PrP, a construct whose inefficient signal sequence mimics the lower translocation efficiency seen for PrP during ER stress (Rane et al., 2008). To stabilize the non-translocated population of lfn-PrP, we also briefly inhibited proteasome function (as might also occur during prion infection; Kristiansen et al., 2007). As with the <sup>C<sup>tm</sup></sup>PrP-favoring constructs, lfn-PrP also caused alterations in lysosomal morphology (in MgrnΔR-expressing cells) that were largely normalized in cells overexpressing Mgrn (Figure 5B). Interestingly, little or no effect was seen for lfn-PrP in the absence of proteasome inhibition where it is degraded highly efficiently (data not shown). Thus, multiple situations that result in either partial and/or transient exposure of PrP to the cytosolic environment at elevated levels lead to alterations in lysosomal morphology that can be rescued upon coexpression of Mgrn, but not MgrnΔR. Importantly, the constructs used for this analysis (e.g., PrP(A117V) and lfn-PrP) lead to more modest phenotypes than the exaggerated situations with GFP-PrP aggregates or SA-PrP, further supporting a direct correlation between the extent of cytosolic PrP exposure and Mgrn dysfunction.

### Analysis in Transgenic Mice

The observation that PrP and Mgrn are expressed in very similar patterns within the central nervous system (Figure S6; Lein et al., 2007) raised the possibility that PrP could influence Mgrn metabolism and/or function in mouse models of PrP-mediated disease involving excessive PrP exposure to the cytosol. To test this idea, we analyzed the status of Mgrn and lysosomes in transgenic mice expressing either human PrP(A117V) or lfn-PrP (Hegde et al., 1998; Rane et al., 2008). As controls, we also analyzed transgenic mice expressing Opn-PrP (Rane et al., 2008), a previously characterized version of PrP in which its signal sequence has been replaced with another signal whose efficiency is slightly higher than wild-type PrP (and hence, does not show increased <sup>C<sup>tm</sup></sup>PrP or cyPrP).

Mgrn immunostaining revealed widespread expression throughout the CNS (Figure S5D), consistent with previous *in situ* data (Figure S6). In Purkinje cells, where expression was especially prominent, reduction in Mgrn staining was observed selectively in HuPrP(A117V) and lfn-PrP mice (Figure 6A). Reduced staining was also observed in the piriform area of the cortex for the HuPrP(A117V) mice but, interestingly, not for the lfn-PrP mice. Conversely, in the subiculum, near the hippocampal region, reduced staining was seen for lfn-PrP but not HuPrP(A117V) mice. In the case of Purkinje cells, we could be certain that lack of staining was not due to the loss of cells, since the cells were clearly present as judged not only by their characteristic morphology but also by costaining with the Purkinje cell marker Calbindin (Figure S7). In the other brain regions, we cannot be certain whether the reduced staining is due to selective cell loss or altered expression. It is noteworthy that in the Opn-PrP brain, no changes in Mgrn staining relative to nontransgenic mice were observed in any brain region in either young or old mice.

At this point, we do not know whether the reduced staining represents reduced protein levels (due perhaps to codegradation of Mgrn upon interaction with PrP) or reduced immunoreactivity due to sequestration. While punctate staining is seen in cell areas lacking the expected diffuse Mgrn staining pattern, we cannot be certain that these represent mislocalized or aggregated Mgrn since similar autofluorescent structures (seen with preimmune samples) confound the interpretation. It should be noted that differences in Mgrn levels were not detected by immunoblotting of brain lysates (data not shown), consistent with the region-selective effects observed by immunohistochemistry.

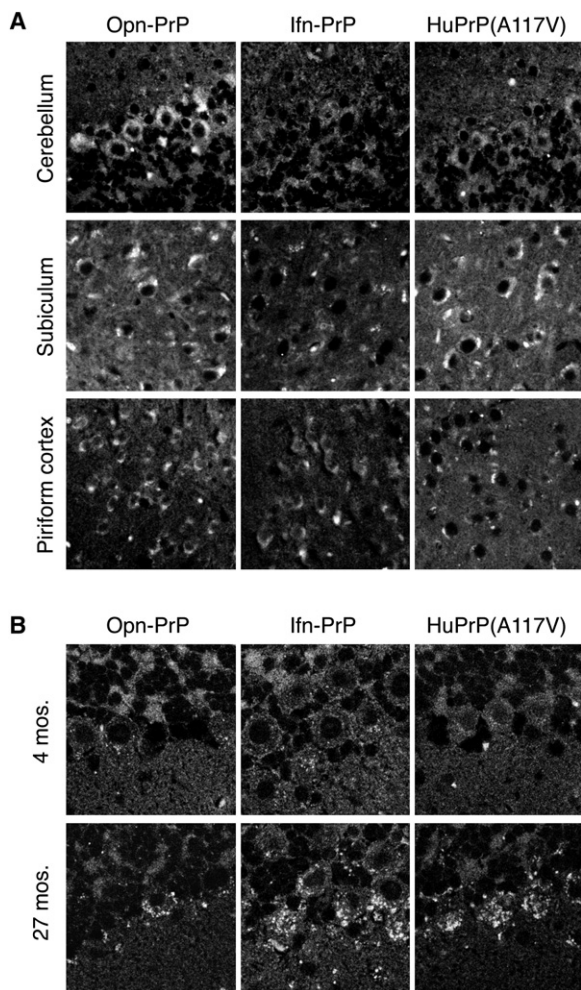


**Figure 6. Alterations in Mgrn and Lysosomes in PrP Mutant Mice**

(A) Age-matched brain sections from the indicated transgenic mice (27 months old) were immunostained with  $\alpha$ -Mgrn serum. Three regions of the brain (see Figure S6) are shown. Note reduced Mgrn staining in Purkinje cells of the cerebellum in HuPrP(A117V) and Ifn-PrP mice, in cells of the subiculum region near the hippocampus of Ifn-PrP mice, and in cells of the piriform cortex of HuPrP(A117V) mice. On histologic sections, Mgrn typically displays diffuse cytosolic staining with nuclear exclusion (see Figure S5). Note that fixation, sectioning, and staining of all sections being compared were performed in parallel, and that imaging conditions were identical among samples.

(B) Age-matched brain sections from the indicated transgenic mice were immunostained with anti-Cathepsin D antibody. The cerebellum is shown. Note enhanced accumulation of Cathepsin D in Purkinje cells of the cerebellum in HuPrP(A117V) and Ifn-PrP mice; this is more than the age-dependent accumulation seen in Opn-PrP mice at 27 months. By contrast to the aged mice, levels of Cathepsin D expression were comparable in 4-month-old transgenic mice.

To examine lysosomal morphology, we analyzed Purkinje cells by staining for the lysosomal enzyme Cathepsin D (CatD). These cells were chosen because they were conclusively identifiable, showed clearly altered Mgrn staining in both HuPrP(A117V) and Ifn-PrP mice, and had not degenerated. Remarkably, a qualitatively obvious increase in CatD staining was seen selectively in the mice that also showed altered Mgrn staining (Figure 6B).

Interestingly, this effect was age dependent, as no changes in CatD staining were observed in any of the mice at 4 months of age. Thus, mouse models of cytosolic PrP exposure, including a naturally occurring human disease mutation (HuPrP(A117V)), result in altered Mgrn expression (or localization) in an age-dependent and cell type-dependent manner. In at least one cell type, altered Mgrn expression is correlated with aberrant lysosomal morphology as was seen in cultured cells.

### Rescue from Functional Mgrn Depletion by Preventing Exposure of PrP to the Cytosol

The data so far indicate that upon cytosolic exposure, PrP can interact with and functionally titrate Mgrn to cause cellular dysfunction. However, the forms of PrP implicated in this mechanism ( $C^{tm}$ PrP and cyPrP) are made at very low levels, even for disease-causing mutations that favor their generation. This raised the crucial question of whether such minor populations of PrP are realistically capable of titrating cellular Mgrn. We therefore quantified Mgrn in brain and found its level to be  $\sim 66$  pmol per gram total brain protein (Figure S8A). By contrast, several studies have carefully determined PrP levels in normal brain to be at least 2 nmol (Pan et al., 1992) and up to  $\sim 6$  nmol (Bendheim et al., 1988) per gram (i.e.,  $\sim 70$ – $200$   $\mu$ g PrP per gram total protein). Given that PrP and Mgrn share very similar patterns of expression in brain (Figure S6), their molar ratio in most cells will be between  $\sim 30$ :1 to 90:1. This means that as little as 1%–2% of PrP exposed to the cytosol may be sufficient to titrate Mgrn. Importantly,  $C^{tm}$ PrP in brain of transgenic mice expressing wild-type PrP represents  $\sim 1\%$  of total PrP, while  $C^{tm}$ PrP in PrP(A117V) mice represents  $\sim 6\%$  of total (Figure S8B). Thus,  $C^{tm}$ PrP exceeds Mgrn on a molar basis for PrP(A117V), but not wild-type PrP.

While the quantification indicates that  $C^{tm}$ PrP levels in disease-causing mutants are sufficient to titrate Mgrn, we sought to test this directly. For this, we took advantage of the observation that  $C^{tm}$ PrP generation by these mutants depends critically on a slight but detectable inefficiency of the PrP signal sequence. Thus, replacing the PrP signal sequence with a more efficient signal (from either Prolactin [Prl] or Osteopontin [Opn]) reduces  $C^{tm}$ PrP levels to near wild-type for mutants such as AV3 and A117V (Kim and Hegde, 2002). Remarkably, Prl-AV3 (the Prl signal fused to the AV3 mutant of PrP) when expressed in cultured cells does not cause the Mgrn-dependent enlarged lysosomal phenotype seen with AV3 (Figure 7A). A similar rescue of the lysosomal phenotype was seen with Opn-HuPrP(A117V) compared to HuPrP(A117V) (Figure 7B).

Analysis of transgenic mice overexpressing (at  $\sim 4\times$  normal; Table S1) Prl-AV3 and Opn-PrP(A117V) showed that Mgrn levels remain detectable throughout the life of the animals (Figures 7C and 7D). Because these mice still contain the pathogenic mutation, differing only in the levels of  $C^{tm}$ PrP, this form indeed appears to be responsible for Mgrn titration and a substantial part of the neurodegenerative phenotype. Thus, while  $C^{tm}$ PrP is only a minor isoform of PrP, its selective elimination alleviates the Mgrn-dependent phenotype in cell culture (Figures 7A and 7B) and Mgrn depletion in mice (Figures 7C and 7D). We therefore conclude that very small amounts of cytosolically exposed PrP are sufficient to influence Mgrn function and contribute to disease.

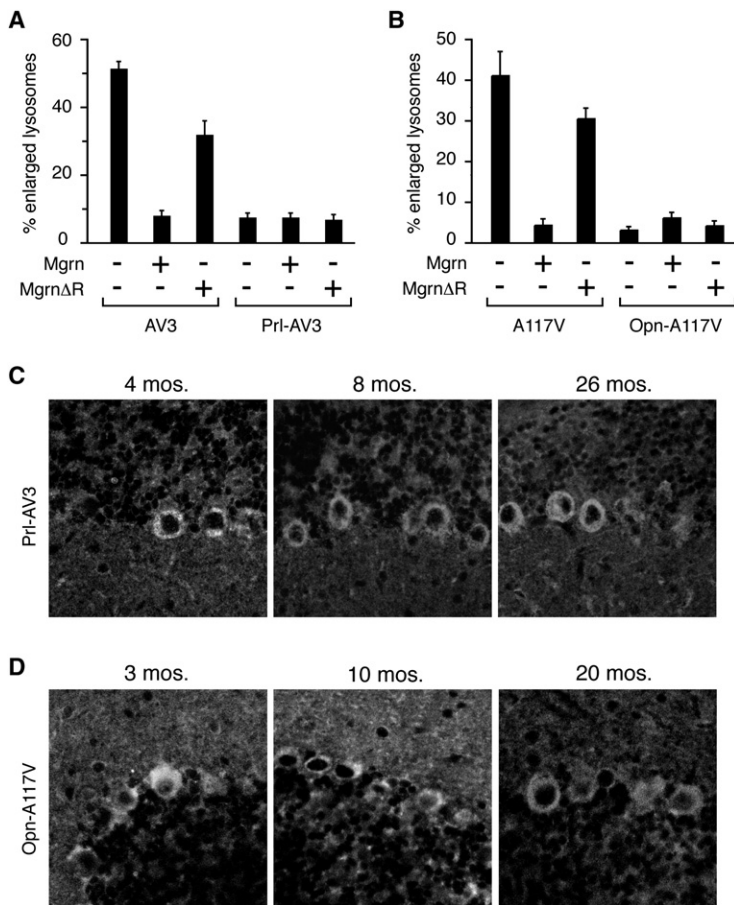


**Figure 7. Selective  $C^{tm}PrP$  Reduction Rescues Mgrn Depletion in Cells and Mice**

(A and B) HeLa cells cotransfected with various PrP constructs and either empty vector, Mgrn, or MgrnΔR were analyzed for lysosomal morphology. The percent of enlarged lysosomes is plotted (mean  $\pm$  SD). The Mgrn-dependent lysosomal phenotypes seen with PrP(AV3) and HuPrP(A117V) are not seen with PrI-PrP(AV3) or Opn-HuPrP(A117V).

(C and D) Brain sections from PrI-PrP(AV3) and Opn-HuPrP(A117V) transgenic mice (lines 6 and 33, respectively) at the indicated ages were immunostained for Mgrn. Normal levels of Mgrn expression in Purkinje cells were observed throughout life in both cases, in contrast to HuPrP(A117V) mice (Figure 6A).

a more efficient signal sequence that acts to selectively minimize PrP exposure to the cytosol. We therefore conclude that inappropriate interaction between cytosolically exposed PrP and Mgrn contributes to the neurodegenerative phenotype in at least a subset of diseases associated with aberrant PrP metabolism. These findings provide a qualitatively new direction for understanding neurodegeneration caused by PrP and raise a wide range of questions for future studies.

Among the various naturally occurring diseases caused by PrP, our findings most directly relate to two subsets of familial cases. One class of mutations within the central hydrophobic domain (P105L, G114V, A117V, G131V, S132I, and A133V) increase the hydrophobicity of this region and likely lead to increased generation of  $C^{tm}PrP$  (as judged by in vitro assays; Hegde et al., 1998; Kim and Hegde, 2002).

The other class includes two premature stop codon mutants (at residues 145 and 160) that seem to display reduced translocation into the ER, thereby generating increased cyPrP (Zanusso et al., 1999; Heske et al., 2004). These diseases may not be transmissible (Tateishi and Kitamoto, 1995; Tateishi et al., 1996; Hegde et al., 1999) and are not “prion” diseases in the true sense; rather, they are better viewed as protein-folding diseases caused by aberrant PrP. Thus, an important question is how our findings might relate to either other familial PrP-mediated diseases or the transmissible prion diseases. The answer to these questions awaits further studies but depends on the extent to which PrP (in particular the N terminus) is ever exposed to the cytosol during the course of disease pathogenesis.

Due to a slightly inefficient signal sequence, even wild-type PrP transits through the cytosol to a small ( $\sim$ 10% of total synthesized PrP) but detectable extent en route to its proteasomal degradation (Rane et al., 2004; Levine et al., 2005; Ma and Lindquist, 2001; Yedidia et al., 2001). Importantly, the molar ratio of PrP to Mgrn in brain ( $\sim$ 30:1 to 90:1) means that as little as 2% of total PrP is equimolar to cellular Mgrn levels. Furthermore, routing of PrP through the cytosol is increased during ER stress due to its reduced translocation into the ER (Kang et al., 2006; Orsi et al., 2006). One implication of these observations is that there is always a *potential opportunity* for Mgrn to interact with PrP, and conditions that enhance this potential might contribute to neurodegeneration via Mgrn sequestration. This could happen

## DISCUSSION

This study elucidates a novel interaction between two disease-causing isoforms of PrP ( $C^{tm}PrP$  and cyPrP) and the putative ubiquitin ligase Mgrn, a protein whose absence leads to spongiform neurodegeneration. In cultured cell systems, the interaction between cytosolically exposed PrP and Mgrn leads to a lysosomal morphology phenotype comparable to that seen upon siRNA-mediated depletion of Mgrn. The relocalization of Mgrn in these cells and the ability to rescue the altered lysosomal phenotype with functional Mgrn (but not a catalytically inactive mutant) argues strongly for functional depletion of Mgrn activity upon its interaction with PrP. Accordingly, these same cytosolically exposed PrP constructs had no effect on lysosomal morphology in a cell type lacking Mgrn. The interaction between PrP and Mgrn was specific since aggregates formed by another neurodegeneration-causing protein (Htt) or PrP aggregates lacking the octapeptide repeats neither interacted with Mgrn nor led to the lysosomal phenotype. Analogous effects on Mgrn immunoreactivity and lysosomal morphology were seen in selected cell types of transgenic mouse models of cytosolically exposed PrP. One of these mouse models corresponds to a naturally occurring mutation (PrP(A117V)) associated with Gerstmann-Straussler-Shienker disease (Hsiao et al., 1991). Remarkably, the Mgrn depletion caused by this mutant could be rescued by

in any of several ways that might be relevant to both genetic and transmissible prion diseases.

For example, transmissible prion diseases are accompanied by both ER stress (Hetz and Soto, 2006; Rane et al., 2008) and reduced proteasome activity (Kristiansen et al., 2007), possibly allowing cyPrP to be both elevated and stabilized. Consistent with such a model, Mgrn was seen to be affected in the Iln-PrP transgenic mice designed to mimic the reduced translocation that might occur during transmissible prion disease. Familial mutants that act via generation of transmissible prions (e.g., E200K or D178N) could act by a similar indirect manner. In addition, if PrP<sup>Sc</sup> were to ever access the cytosol as has been proposed (Kristiansen et al., 2007), it too could sequester Mgrn in much the same way as our artificial cytosolic PrP aggregates. In other PrP-mediated diseases, the mutations may directly enhance the interaction with Mgrn, as might be the case with octapeptide repeat insertions. This could allow even the normally small amount of cytosolic PrP to contribute to neurodegeneration. Conversely, deletion of repeats seems to attenuate transmissible prion disease severity (Flechsigs et al., 2000), perhaps because one adverse downstream event (Mgrn interaction) is minimized. Intriguingly, mice expressing PrP lacking all ORs do not show typical spongiform pathology in the CNS upon prion infection (Flechsigs et al., 2000). Thus, via a combination of different mechanisms, it is plausible that an interaction between Mgrn and cytosolically exposed PrP may be a contributing factor in many or all PrP-mediated neurodegenerative diseases, and not just those involving C<sup>tm</sup>PrP. Each of these hypotheses merit further examination to see if cytosolically exposed PrP is indeed generated and/or stabilized in sufficient amounts to influence Mgrn localization and function. Because PrP is a very abundant protein (and often accumulates to many-fold higher levels during disease), even relatively small proportions of it (a few percent) in the cytosol would be sufficient to affect the comparatively low abundance of Mgrn.

Depletion of Mgrn by cytosolically exposed PrP is likely to be a *contributing* factor, and not the sole downstream event, leading to neurodegeneration. This supposition is based on the fact that PrP-mediated neurodegeneration in mice can be significantly more severe than simply knocking out Mgrn (where pathology is observed at 6–12 months; He et al., 2003). However, there are several possible ways in which an inappropriate interaction with PrP is actually more detrimental than a knockout. One way is if acute or adult-onset depletion of Mgrn precludes compensatory mechanisms that are otherwise initiated in a germline knockout. Another is if cytosolic PrP partially codepletes factors that associate with Mgrn. Although Mgrn is largely dispensable, it may associate with other factors whose loss (even partially) is far more detrimental. One candidate is Tsg101 (Kim et al., 2007), a key component of the ESCRT machinery involved in endolysosomal trafficking (Hurley, 2008). By depleting this and/or other ESCRT factors, the PrP-Mgrn interaction could more severely influence lysosomal trafficking and cellular function than simply deleting Mgrn. Thus, while it is likely that most instances of PrP-mediated neurodegeneration will involve multiple downstream pathways leading to cellular dysfunction, it is nonetheless plausible that the Mgrn interaction could play a much more central role than might initially appear based on the rela-

tively mild phenotype of Mgrn null mice. If this is the case, one might predict that prion infection of Mgrn null mice would lead to a much milder phenotype than otherwise expected upon PrP<sup>Sc</sup> accumulation.

Further insight into the mechanism of neuronal dysfunction may come from a better understanding of Mgrn function. At present, the substrates or site(s) of action for this putative ubiquitin ligase are unknown. It has been suggested on the basis of genetic evidence that Mgrn functions in the same pathway as Attractin, a cell-surface receptor implicated in melanocortin signaling (He et al., 2003). In another study, Mgrn was shown to interact with and ubiquitinate Tsg101 to influence endosomal trafficking (Kim et al., 2007). This latter result could mean that Mgrn influences receptor recycling and/or downregulation via receptor monoubiquitination, an increasingly common trafficking signal in the endolysosomal system (Piper and Luzio, 2007). This would place Mgrn in the ubiquitous and essential pathway of ubiquitin-dependent trafficking of membrane proteins, consistent with the observed localization pattern on intracellular vesicles. However, its role in endolysosomal pathways would presumably be nonessential or functionally redundant since the phenotype of Mgrn null mice is restricted to a small subset of cells despite rather widespread expression (He et al., 2003). Such functional redundancy could explain why despite widespread expression of both cyPrP and C<sup>tm</sup>PrP (both within and outside the nervous system), the phenotype appears to be relatively focal (Hegde et al., 1998; Ma et al., 2002; Rane et al., 2008). Indeed, in cultured cells that lack Mgrn expression, neither cyPrP aggregates nor C<sup>tm</sup>PrP lead to alterations in lysosomal morphology. Thus, one explanation for the selectivity of cell death in prion diseases may involve interacting partners, such as Mgrn, whose expression or functional importance is restricted. This would mean that cyPrP and C<sup>tm</sup>PrP are not intrinsically cytotoxic but depend critically on their cellular context. It will therefore be important not only to identify other potential interacting partners of cytosolically exposed PrP but to clearly delineate their expression and function to elucidate how they might contribute to neurodegeneration.

## EXPERIMENTAL PROCEDURES

### Constructs and Antibodies

All of the PrP-derived constructs have been described before (Hegde et al., 1998; Rane et al., 2008; Kim and Hegde, 2002; see Supplemental Experimental Procedures). The FP-PrP<sub>x-231</sub> constructs and Mgrn deletion constructs were generated by standard cloning techniques (see Supplemental Experimental Procedures). SA-PrP is characterized in Figure S2. GFP-tagged Htt exon 1 containing 103 glutamines was a gift of L. Greene (NIH). Antibodies were from the following sources: 3F4 and 6D11 mouse monoclonal against PrP (Signet); Calbindin D28k (Sigma); Cathepsin D (Santa Cruz Biotechnology). The GFP and RFP antibodies were raised against the full-length recombinant proteins. Anti-GFP reacts to all GFP-derived FPs (e.g., CFP, Cerulean, YFP, etc.), but not RFP (data not shown). Rabbit anti-Mgrn was raised against purified His-tagged full-length Mgrn.

### Cell Culture and Imaging

Culture of HeLa and N2a cells, transient transfections, preparation of stable cell lines, immunofluorescent staining, and fluorescence microscopy of fixed and live cells were as done previously (Rane et al., 2004, 2008). For quantitative

analyses and comparisons between multiple samples, images were collected using identical excitation and detection settings within the linear range of the photomultiplier tube without saturating pixels. Immunohistochemistry was with minor modifications of earlier methods (Rane et al., 2008; see Supplemental Experimental Procedures).

#### Analysis of Lysosomes

Transfected cells were stained with 500 nM LysoTracker Red DND-99 (Molecular Probes) for 30 min at 37°C, rinsed with cold 1 × PBS (4°C), and fixed with 3.7% formaldehyde in PBS for 10 min at room temperature before imaging. Random fields of transfected cells (identified by GFP coexpression) were chosen blindly (without visualization of lysosomal staining), and images were collected in both the GFP and LysoTracker channels. Five or six fields, each containing at least four transfected cells, were imaged. Using ImageJ, the lysosome images were converted to black and white images using the threshold function, and the lysosome diameter for each lysosome was manually measured. The data were tabulated in Microsoft Excel, which was used to generate the histograms and perform statistical analyses by the Student's two-tailed t test.

#### Semipermeabilization Assays

Semipermeabilization and imaging to detect interactions between proteins (e.g., Figure 1) were done as described previously (Lorenz et al., 2006; characterized in Figure S1). Biochemical fractionation by selective detergent extraction has been described (Levine et al., 2005; see Supplemental Experimental Procedures).

#### Knockdowns with siRNA

ON-TARGETplus SMARTpool siRNAs against Mgrn and GFP (catalog# L-022620-00-0005 and D-001300-01-20; Thermo Scientific Dharmacon products) were transfected using Lipofectamine 2000 (Invitrogen) following the manufacturer's instructions. Constructs to be analyzed were transfected 48 hr after siRNA treatment, and the cells visualized 24 hr later.

#### Peptide-Binding Assay

A synthetic peptide containing the OR sequence, followed by three glycines and a cysteine (PHGGGWGQGGGC), was coupled to Sulfo-Link beads (Pierce). Cytosol for pull-down experiments was generated from 10 cm dishes of transfected N2a cells. Cell lysate was prepared in 1.5 ml of KHM (110 mM KAc, 20 mM HEPES, pH 7.2, 2 mM MgAc<sub>2</sub>) containing 200 μg/ml digitonin. Debris was removed by centrifugation, and 1250 μl was incubated with 50 μl of beads (either sepharose or peptide-conjugated sepharose) for 2 hr at 4°C. The beads were washed several times with KHM containing 100 μg/ml digitonin prior to elution with SDS.

#### Brain Lysate-Binding Assay

Approximately 3 mg purified recombinant Mgrn and BSA fraction V (Sigma) were immobilized on ~1 ml CnBr activated sepharose (Amersham Pharmacia). Two hundred microliters of total hamster brain homogenate (10% w/v) prepared in PBS containing 0.5% Triton X-100, 0.5% sodium deoxycholate was clarified by centrifugation and diluted with 1620 μl of KHM containing 100 μg/ml digitonin. This lysate was equally divided and incubated with 50 μl of each of the immobilized-protein beads for 2 hr at 4°C. The beads were then washed with KHM containing 100 μg/ml digitonin, after which they were eluted in SDS.

#### Biochemical Analyses In Vitro and in Cells

In vitro translocation assays, pulse-chase analyses, glycosidase sensitivity, and immunofluorescence of PrP (and related constructs) employed previously described methods (Hegde et al., 1998; Rane et al., 2004; Kang et al., 2006).

#### Transgenic Mice

I<sup>fln</sup>-PrP and Opn-PrP transgenic mice have been described (Rane et al., 2008). Transgenic mice expressing HuPrP(A117V), Opn-HuPrP(A117V), and Prl-PrP(AV3) mice were generated as described before (Hegde et al., 1999) and will be characterized in greater detail elsewhere. Transgenic lines 6, 36, and

33 of Prl-PrP(AV3), HuPrP(A117V), and Opn-HuPrP(A117V), respectively, were analyzed (see Table S1).

#### SUPPLEMENTAL DATA

Supplemental Data include Supplemental Experimental Procedures, one table, and eight figures and can be found with this article online at [http://www.cell.com/supplemental/S0092-8674\(09\)00379-1](http://www.cell.com/supplemental/S0092-8674(09)00379-1).

#### ACKNOWLEDGMENTS

We are grateful to N. Rane for providing transgenic mouse tissues and constructs, E. Whiteman for making the initial Mgrn constructs, Y. Abebe for expert animal care, L. Greene and H. Lorenz for constructs and sharing unpublished results, G. Patterson for help with microscopy, and L. DaSilva, G. Mardones, and P. Burgos for advice and reagents. This work was supported by the Intramural Research Program of the NICHD at the National Institutes of Health.

Received: July 11, 2008

Revised: January 13, 2009

Accepted: March 20, 2009

Published: June 11, 2009

#### REFERENCES

- Aguzzi, A., Heikenwalder, M., and Polymenidou, M. (2007). Insights into prion strains and neurotoxicity. *Nat. Rev. Mol. Cell Biol.* 8, 552–561.
- Bendheim, P.E., Potempska, A., Kascsak, R.J., and Bolton, D.C. (1988). Purification and partial characterization of the normal cellular homolog of the scrapie agent protein. *J. Infect. Dis.* 158, 1198–1208.
- Brandner, S., Isenmann, S., Raeber, A., Fischer, M., Sailer, A., Kobayashi, Y., Marino, S., Weissmann, C., and Aguzzi, A. (1996). Normal host prion protein necessary for scrapie-induced neurotoxicity. *Nature* 379, 339–343.
- Chakrabarti, O., Ashok, A., and Hegde, R.S. (2009). Prion protein biosynthesis and its emerging role in neurodegeneration. *Trends Biochem. Sci.* Published online May 15, 2009. 10.1016/j.tibs.2009.03.001.
- Chesebro, B., Trifilo, M., Race, R., Meade-White, K., Teng, C., LaCasse, R., Raymond, L., Favara, C., Baron, G., Priola, S., et al. (2005). Anchorless prion protein results in infectious amyloid disease without clinical scrapie. *Science* 308, 1435–1439.
- Chiesa, R., Piccardo, P., Quaglio, E., Drisaldi, B., Si-Hoe, S.L., Takao, M., Ghetti, B., and Harris, D.A. (2003). Molecular distinction between pathogenic and infectious properties of the prion protein. *J. Virol.* 77, 7611–7622.
- Collinge, J., and Clarke, A.R. (2007). A general model of prion strains and their pathogenicity. *Science* 318, 930–936.
- Dahlmann, B. (2007). Role of proteasomes in disease. *BMC Biochem.* 8 (Suppl 1), S3.
- Flechsigs, E., Shmerling, D., Hegyi, I., Raeber, A.J., Fischer, M., Cozzio, A., von Mering, C., Aguzzi, A., and Weissmann, C. (2000). Prion protein devoid of the octapeptide repeat region restores susceptibility to scrapie in PrP knockout mice. *Neuron* 27, 399–408.
- He, L., Lu, X.Y., Jolly, A.F., Eldridge, A.G., Watson, S.J., Jackson, P.K., Barsh, G.S., and Gunn, T.M. (2003). Spongiform degeneration in mahoganoid mutant mice. *Science* 299, 710–712.
- Hegde, R.S., Mastrianni, J.A., Scott, M.R., DeFea, K.A., Tremblay, P., Torchia, M., DeArmond, S.J., Prusiner, S.B., and Lingappa, V.R. (1998). A transmembrane form of the prion protein in neurodegenerative disease. *Science* 279, 827–834.
- Hegde, R.S., Tremblay, P., Groth, D., DeArmond, S.J., Prusiner, S.B., and Lingappa, V.R. (1999). Transmissible and genetic prion diseases share a common pathway of neurodegeneration. *Nature* 402, 822–826.
- Heske, J., Heller, U., Winklhofer, K.F., and Tatzelt, J. (2004). The C-terminal globular domain of the prion protein is necessary and sufficient for import into the endoplasmic reticulum. *J. Biol. Chem.* 279, 5435–5443.

- Hetz, C.A., and Soto, C. (2006). Stressing out the ER: a role of the unfolded protein response in prion-related disorders. *Curr. Mol. Med.* 6, 37–43.
- Hsiao, K.K., Cass, C., Schellenberg, G.D., Bird, T., Devine-Gage, E., Wisniewski, H., and Prusiner, S.B. (1991). A prion protein variant in a family with the telencephalic form of Gerstmann-Straussler-Scheinker syndrome. *Neurology* 41, 681–684.
- Hurley, J.H. (2008). ESCRT complexes and the biogenesis of multivesicular bodies. *Curr. Opin. Cell Biol.* 20, 4–11.
- Kang, S.W., Rane, N.S., Kim, S.J., Garrison, J.L., Taunton, J., and Hegde, R.S. (2006). Substrate-specific translocational attenuation during ER stress defines a pre-emptive quality control pathway. *Cell* 127, 999–1013.
- Kim, B.Y., Olzmann, J.A., Barsh, G.S., Chin, L.S., and Li, L. (2007). Spongiform neurodegeneration-associated E3 ligase Mahogunin ubiquitylates TSG101 and regulates endosomal trafficking. *Mol. Biol. Cell* 18, 1129–1142.
- Kim, S.J., and Hegde, R.S. (2002). Cotranslational partitioning of nascent prion protein into multiple populations at the translocation channel. *Mol. Biol. Cell* 13, 3775–3786.
- Kristiansen, M., Deriziotis, P., Dimcheff, D.E., Jackson, G.S., Ovaa, H., Naumann, H., Clarke, A.R., van Leeuwen, F.W., Menendez-Benito, V., Dantuma, N.P., et al. (2007). Disease-associated prion protein oligomers inhibit the 26S proteasome. *Mol. Cell* 26, 175–188.
- Lein, E.S., Hawrylycz, M.J., Ao, N., Ayres, M., Bensinger, A., Bernard, A., Boe, A.F., Boguski, M.S., Brockway, K.S., Byrnes, E.J., et al. (2007). Genome-wide atlas of gene expression in the adult mouse brain. *Nature* 445, 168–176.
- Levine, C.G., Mitra, D., Sharma, A., Smith, C.L., and Hegde, R.S. (2005). The efficiency of protein compartmentalization into the secretory pathway. *Mol. Biol. Cell* 16, 279–291.
- Lorenz, H., Hailey, D.W., and Lippincott-Schwartz, J. (2006). Fluorescence protease protection of GFP chimeras to reveal protein topology and subcellular localization. *Nat. Methods* 3, 205–210.
- Ma, J., and Lindquist, S. (2001). Wild-type PrP and a mutant associated with prion disease are subject to retrograde transport and proteasome degradation. *Proc. Natl. Acad. Sci. USA* 98, 14955–14960.
- Ma, J., Wollmann, R., and Lindquist, S. (2002). Neurotoxicity and neurodegeneration when PrP accumulates in the cytosol. *Science* 298, 1781–1785.
- Mallucci, G., Dickinson, A., Linehan, J., Klöhn, P.C., Brandner, S., and Colinge, J. (2003). Depleting neuronal PrP in prion infection prevents disease and reverses spongiosis. *Science* 302, 871–874.
- Orsi, A., Fioriti, L., Chiesa, R., and Sitia, R. (2006). Conditions of endoplasmic reticulum stress favor the accumulation of cytosolic prion protein. *J. Biol. Chem.* 281, 30431–30438.
- Pan, K.N., Stahl, N., and Prusiner, S.B. (1992). Purification and properties of the cellular prion protein from Syrian hamster brain. *Protein Sci.* 1, 1343–1352.
- Piper, R.C., and Luzio, J.P. (2007). Ubiquitin-dependent sorting of integral membrane proteins for degradation in lysosomes. *Curr. Opin. Cell Biol.* 19, 459–465.
- Rane, N.S., Yonkovich, J.L., and Hegde, R.S. (2004). Protection from cytosolic prion protein toxicity by modulation of protein translocation. *EMBO J.* 23, 4550–4559.
- Rane, N.S., Kang, S.W., Chakrabarti, O., Feigenbaum, L., and Hegde, R.S. (2008). Reduced translocation of nascent prion protein during ER stress contributes to neurodegeneration. *Dev. Cell* 15, 359–370.
- Tateishi, J., and Kitamoto, T. (1995). Inherited prion diseases and transmission to rodents. *Brain Pathol.* 5, 53–59.
- Tateishi, J., Kitamoto, T., Hoque, M.Z., and Furukawa, H. (1996). Experimental transmission of Creutzfeldt-Jakob disease and related diseases to rodents. *Neurology* 46, 532–537.
- Yedidia, Y., Horonchik, L., Tzaban, S., Yanai, A., and Taraboulos, A. (2001). Proteasomes and ubiquitin are involved in the turnover of the wild-type prion protein. *EMBO J.* 20, 5383–5391.
- Zanusso, G., Petersen, R.B., Jin, T., Jing, Y., Kanoush, R., Ferrari, S., Gambetti, P., and Singh, N. (1999). Proteasomal degradation and N-terminal protease resistance of the codon 145 mutant prion protein. *J. Biol. Chem.* 274, 23396–23404.

Cell, Volume 137

## Supplemental Data

# Functional Depletion of Mahogunin by Cytosolically Exposed Prion Protein Contributes to Neurodegeneration

Oishee Chakrabarti and Ramanujan S. Hegde

### Supplemental Experimental Procedures

**Constructs, antibodies and reagents** – The following PrP-derived constructs are based on hamster PrP and have been described previously (Hegde et al., 1998; Kim and Hegde, 2002; Rane et al., 2008): Ifn-PrP, Opn-PrP, PrP(A117V), PrP(AV3), and PrI-PrP(AV3). HuPrP(A117V) encodes Human PrP containing the A117V mutation. Opn-HuPrP(A117V) encodes the signal sequence from Osteopontin (Opn) fused to HuPrP(A117V) (Kim and Hegde, 2002). FP-PrP<sub>x-231</sub> constructs were generated by inserting the respective PCR fragments of PrP in FP expression constructs from Clontech. Mouse Mgrn cDNA (from ATCC) was subcloned into mammalian (pCNDA3.1, Invitrogen), bacterial (pRSETA), or FP expression vectors. Mgrn deletion constructs were generated by standard cloning techniques to remove codons 2-252 (Mgrn $\Delta$ N), 252-325 (Mgrn $\Delta$ R), or 254-533 (Mgrn $\Delta$ C). Mgrn $\Delta$ 1-147, Mgrn $\Delta$ 1-199 and Mgrn $\Delta$ 1-251 constructs were generated by standard cloning techniques to remove codons 2-147, 2-199 and 2-251, respectively of Mgrn. Mgrn<sub>200-250</sub> was generated by inserting corresponding PCR fragment of Mgrn in mCer expression construct from Clontech. SA-PrP was generated by replacing the hydrophobic domain of hamster PrP (residues AGAVVGGGLGGYMLGSAM) with the transmembrane domain of human asialoglycoprotein receptor (LLLLSLGLSLLLLVVVVCVIG) in a PrP construct that lack its N-terminal signal sequence. L9R-3AV PrP was generated by site-directed mutagenesis to replace leucine at codon 9 with arginine in PrP(AV3) to generate a construct similar to that described previously (Stewart et al., 2001). GFP-tagged Htt exon 1 containing 103 glutamines was a gift of L. Greene (NIH). Antibodies were from the following sources: 3F4 and 6D11 mouse monoclonal against PrP (Signet); Calbindin D28k (Sigma); Cathepsin D (Santa Cruz Biotechnology); TRAP $\alpha$  (Fons et al., 2003). The GFP and RFP antibodies were raised against the full length recombinant proteins and confirmed to be specific by western blot, immunoprecipitation, and immunofluorescence. Anti-GFP reacts to all GFP-derived FPs (e.g., CFP, Cerulean, YFP, etc.), but not RFP (data not shown). Rabbit anti-Mgrn was raised against purified His-tagged full length Mgrn expressed in BL21 p(Lys)S cells (Novagen). Pre-immune sera from the same rabbits, prior to immunization were saved for controls. Other reagents and chemicals were obtained from the following companies: MG132 and digitonin (Calbiochem); Sepharose CL-4B (Sigma); Sulfo-Link beads (Pierce).

**Cell Culture** – HeLa and N2a cells were cultured in DMEM containing 10% fetal bovine serum (FBS) at 5% CO<sub>2</sub>. The cells were transfected with Lipofectamine 2000 (Invitrogen). All assays using transiently transfected cells were carried out 24 hours post-transfection. Stable cell lines were generated by selection in Zeocin for 4 weeks, followed by subcloning of individual

colonies. Several individual clones at different expression levels were analyzed. Data are shown for two clones whose levels of expression and growth rates were the same. For confocal microscopic imaging experiments, cells used for live-cell imaging were grown in 35 mm glass bottom microwell dishes (MatTek Corporation), while those to be fixed and immunostained were grown in 8-well Lab-Tek chambered coverglass (Nunc). Biochemical assays were on cells grown in 6-well tissue-culture dishes unless otherwise noted.

**Semi-permeabilization assays** – For imaging interactions between proteins (e.g., Fig. 1) randomly chosen fields of cells were rinsed with 2 ml KHM (110 mM KAc, 20 mM Hepes, pH 7.2, 2mM MgAc<sub>2</sub>) and then put into 1 ml KHM to capture pre-Dig images. The KHM was replaced with 1 ml KHM containing 100 ug/ml digitonin and imaged at 2 min intervals for a total of 20 minutes. Three dishes were imaged for each set of transfections and the complete set of experiments was performed three times to verify all results. Biochemical fractionation (Fig. 1g) was similar to previous methods (Levine et al., 2005): cells were washed with 2 ml KHM and extracted with KHM containing digitonin (at 100 ug/ml; Levine et al., 2005) to generate the soluble cytosolic fraction. The cells were then washed once in KHM and subsequently extracted in 1ml IP buffer (50 mM Hepes, pH 7.4, 100 mM NaCl, 1% Triton X-100) to recover the Triton X-100 wash fraction. The remaining insoluble material (sedimented for 10 min in a microfuge) was dissolved in 1% SDS. Proteins from the soluble and wash fractions were precipitated using 12% Trichloroacetic acid, washed in acetone, and dissolved in SDS prior to analysis.

**Fluorescence microscopy and imaging** – Fluorescence microscopy was performed utilizing LSM510/ConfoCor 2 microscopy system (Zeiss) equipped with an Ar-ion laser (for CFP or GFP excitation with the 458 nm and 488 nm lines, respectively), and a He-Ne laser (for RFP and Alexa-Fluor 594 excitation with the 543 line). Experiments imaging lysosomes were performed using Olympus FluoView FV1000 equipped with with an Ar-ion laser (for GFP excitation with the 488 nm line), and a He-Ne laser (for LysoTracker Red DND-99 excitation with the 543 line). A 40x or 63x 1.4 NA oil immersion objective was used for all imaging. For quantitative analyses and comparisons between multiple samples, images were collected using identical excitation and detection settings. The detector gain settings were chosen to allow imaging of the desired cells within the linear range of the photomultiplier tube without saturating pixels.

Immunofluorescence of cultured cells was as before (Rane et al., 2004). Immunohistochemistry was with slightly modifications of earlier methods (Rane et al., 2008). Briefly, paraffin-embedded 5 µm sagittal brain sections were dewaxed with EZ-DeWax (Biogenex), rinsed with 100% ethanol twice, and rehydrated with continuous flowing water. The sections were then treated for antigen retrieval with citrate-buffer (containing 10 mM sodium citrate, 0.05% Tween-20, pH = 6.0) by incubating in water bath at 100<sup>0</sup>C for 10 minutes. The sections were rinsed with TBS containing 0.025% Triton X-100 and blocked in blocking buffer (containing 0.25% Triton X-100 and 10% serum) for 2 hours at room temperature. Primary antibodies were diluted in blocking buffer (rabbit polyclonal anti-Mgrn and pre-immune serum, both at 1:1000 dilution, Calbindin at 1:500 and Cathepsin D at 1:50 dilution) and incubated with the sections for 2 hours at room temperature. After rinsing with TBS containing 0.025% Triton X-100, the sections were incubated with secondary antibodies (conjugated to Alexa-Fluor 594 or conjugated to Alexa-Fluor 568) for 1 hour at room temperature. After washing, sections were mounted with Vectashield (Vector Laboratories) prior to imaging. Cathepsin D staining used normal rabbit serum for blocking; otherwise fetal bovine serum was used.

**Table S1 - Characteristics of transgenic mice used in this study.**

<b>Transgene<sup>a</sup></b>	<b>Exp. Level<sup>b</sup></b>	<b>Effect on translocation<sup>c</sup></b>	<b>Time to disease<sup>d</sup></b>
Opn-PrP	2X	Reduced <sup>C<sup>tm</sup></sup> PrP & cyPrP	> 600 d
Ifn-PrP	0.2X	Increased cyPrP	~ 100 d
Prl-PrP(AV3) <sub>6</sub>	4X	Close to wild type	~ 600 d
HuPrP(A117V) <sub>36</sub>	2.5X	Increased <sup>C<sup>tm</sup></sup> PrP	~ 550 d
Opn-HuPrPr(A117V) <sub>33</sub>	4X	Close to wild type	> 600 d

<sup>a</sup> The first two lines have been described before (Rane et al., 2008).

<sup>b</sup> Relative to PrP levels in normal Hamster (defined as 1X); Note that due to rapid proteasomal degradation, the steady state expression level of Ifn-PrP is very low (less than 0.1X), but based on mRNA analysis, is estimated to be synthesized at ~0.2X (see Rane et al., 2008).

<sup>c</sup> Based on analyses in vitro from earlier studies (Kim and Hegde, 2002; Rane et al., 2008)

<sup>d</sup> Note that Ifn-PrP, although showing symptoms within weeks after birth, has a normal lifespan (Rane et al., 2008). HuPrP(A117V)<sub>36</sub> develops symptoms at ~18 months, and has slightly shorter lifespan than Opn-HuPrPr(A117V)<sub>33</sub>.

## **Supplemental References**

Fons, R.D., Bogert, B.A., and Hegde, R.S. (2003). Substrate-specific function of the translocon-associated protein complex during translocation across the ER membrane. *J Cell Biol* *160*, 529-539.

Hegde, R.S., Mastrianni, J.A., Scott, M.R., DeFea, K.A., Tremblay, P., Torchia, M., DeArmond, S.J., Prusiner, S.B., and Lingappa, V.R. (1998). A transmembrane form of the prion protein in neurodegenerative disease. *Science* *279*, 827-834.

Kim, S.J., and Hegde, R.S. (2002). Cotranslational partitioning of nascent prion protein into multiple populations at the translocation channel. *Mol Biol Cell* *13*, 3775-3786.

Levine, C.G., Mitra, D., Sharma, A., Smith, C.L., and Hegde, R.S. (2005). The efficiency of protein compartmentalization into the secretory pathway. *Mol Biol Cell* *16*, 279-291.

Rane, N.S., Kang, S.W., Chakrabarti, O., Feigenbaum, L., and Hegde, R.S. (2008). Reduced translocation of nascent prion protein during ER stress contributes to neurodegeneration. *Dev Cell* *15*, 359-370.

Rane, N.S., Yonkovich, J.L., and Hegde, R.S. (2004). Protection from cytosolic prion protein toxicity by modulation of protein translocation. *Embo J* *23*, 4550-4559.

Stewart, R.S., Drisaldi, B., and Harris, D.A. (2001). A transmembrane form of the prion protein contains an uncleaved signal peptide and is retained in the endoplasmic Reticulum. *Mol Biol Cell* *12*, 881-889.

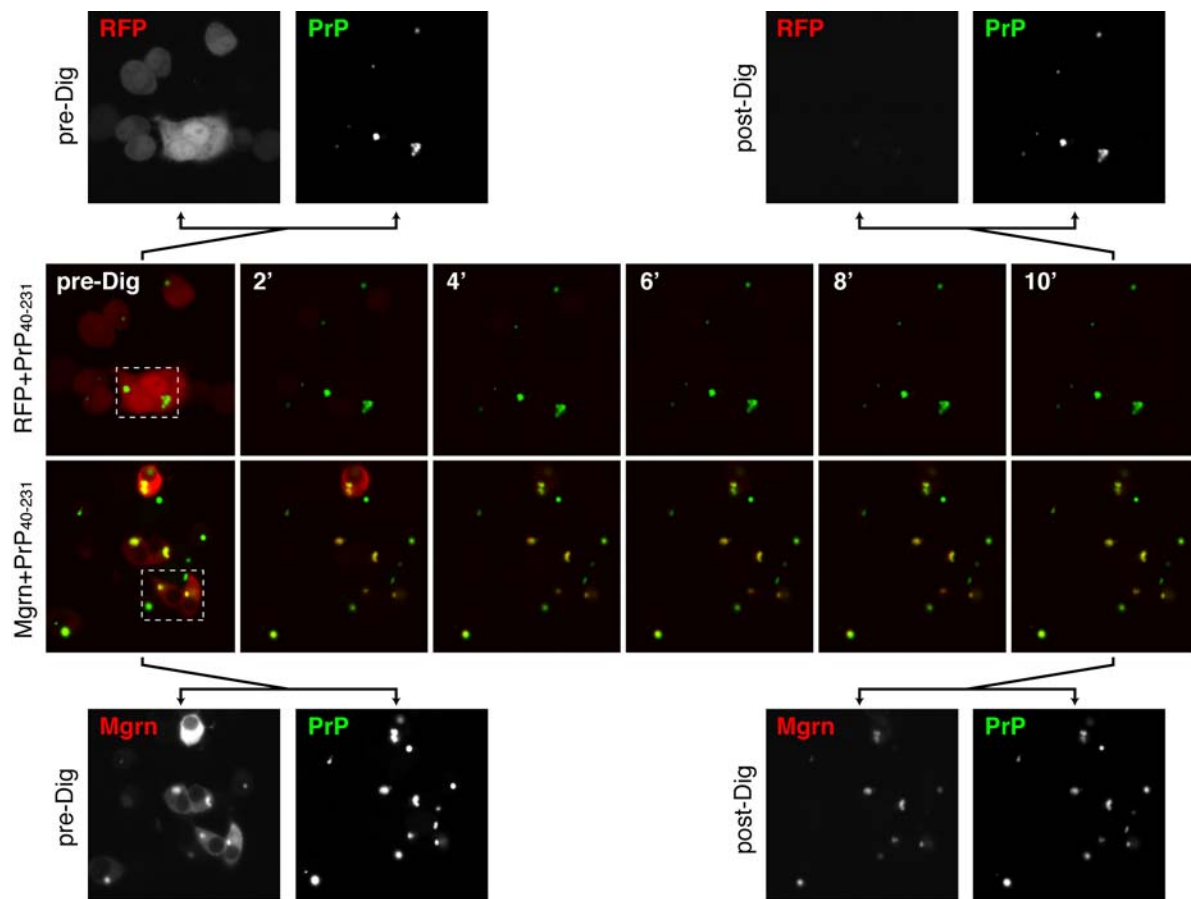


**Fig. S1. Time course of soluble and insoluble protein extraction.** N2a cells co-transfected with CFP-PrP<sub>40-231</sub> (green) and either RFP or Mgrn-RFP (red) were imaged every 2 min during 10 min of digitonin semi-permeabilization. The first image (before semi-permeabilization - 'pre-Dig') and last image ('post-Dig') are also shown as grayscale split images to illustrate complete loss of RFP, but retention of the CFP-PrP(40-231) aggregates. Note that Mgrn-RFP in the aggregates is retained upon permeabilization, indicating co-sequestration by its interaction with CFP-PrP(40-231). Magnified views of the pre-Dig and post-Dig images from the boxed regions are shown in Fig. 1C. All images were captured using the same microscope settings.

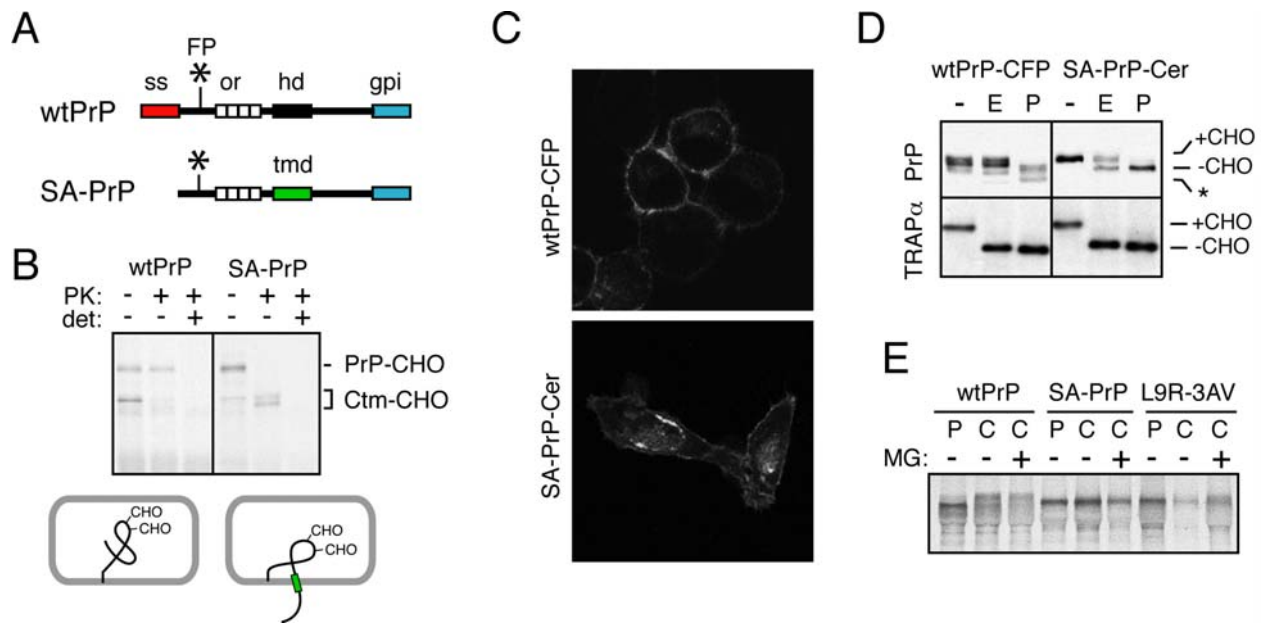


**Fig. S2. Characterization of SA-PrP as a <sup>Ctm</sup>PrP-only construct.** (A) Schematic diagram of wild type PrP and SA-PrP, with key domains indicated: N-terminal signal sequence (red), octapeptide repeats (white), central hydrophobic domain (black), C-terminal GPI signal (blue), and signal anchor (green). The site for fluorescent protein (FP) insertion is indicated (asterisk). (B) In vitro translocation assay for wild type PrP and SA-PrP. Constructs were translated in reactions containing ER microsomes, and their topology assessed by protease protection. Note that essentially all of the glycosylated PrP ('+CHO') is fully protected from proteinase K (PK) digestion, indicating its complete translocation into the microsomes. By contrast, the N-terminus of glycosylated SA-PrP was digested due to its exposure to the cytosol, leaving a protected C-terminal domain ('Ctm'). Thus, SA-PrP is made exclusively in the <sup>Ctm</sup>PrP topology, as indicated below the gel. (C) Localization of SA-PrP-Cer and wtPrP-CFP in stably transfected N2a cells. The same imaging conditions were used for the two constructs, indicating similar expression levels (see panel E below). (D) Total cell lysates from SA-PrP-Cer and wtPrP-CFP cells were digested with Endoglycosidase H (E), PNGase F (P) or left untreated (-) before immunoblotting with antibodies against PrP (top panel) or TRAP $\alpha$ , an ER resident glycoprotein. Positions of glycosylated (+CHO) and unglycosylated (-CHO) PrP are indicated. A presumed lysosomal degradation intermediate of PrP is indicated by the asterisk. (E) Pulse-chase analyses of N2a cells transiently transfected with the indicated constructs performed in the absence or presence of proteasome inhibitor (5  $\mu$ M MG132). Note that in contrast to L9R-3AV (Stewart et al., 2001), neither PrP nor SA-PrP are degraded rapidly or stabilized by proteasome inhibition.

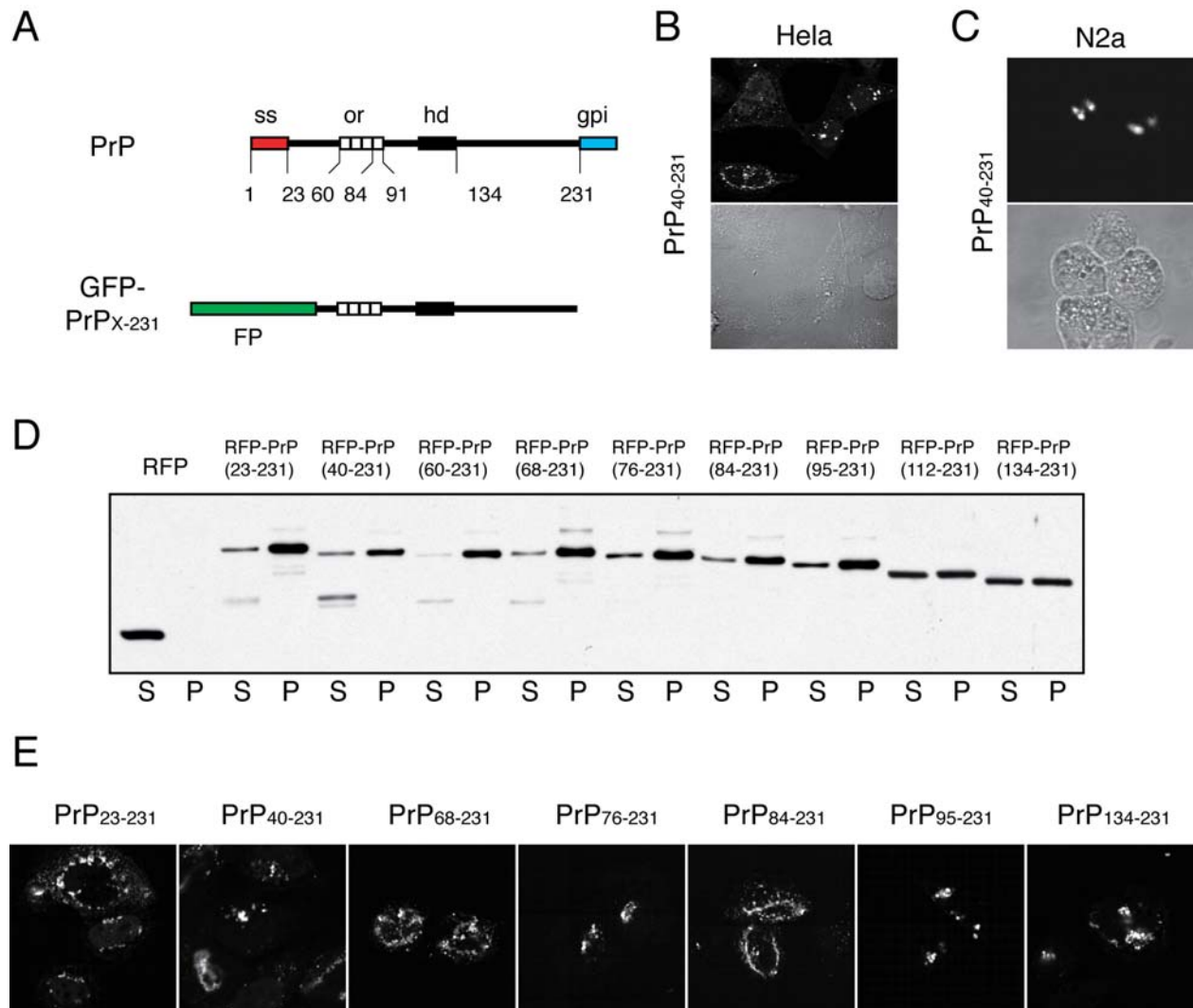


**Fig. S3. Cytosolic GFP-PrP fusions form aggregates in cells.** (A) Line diagram of GFP-PrP fusions relative to wild type PrP. The positions of the N-terminal signal sequence (red), central hydrophobic domain (black), GPI anchoring signal sequence (blue), and octapeptide repeats (white) are indicated. Residue numbers of key landmarks are shown below the sequence. The subscript on PrP indicates the residues fused to the fluorescent protein (FP). (B & C) Localization of GFP-PrP<sub>40-231</sub> upon expression in HeLa and N2a cells. Note that aggregate morphology displayed both cell-to-cell variation and cell type differences. In HeLa cells, aggregates were often more disperse and numerous than N2a cells, where larger, fewer aggregates are typical. Aggregates were seen for various FPs including CFP, GFP, and RFP. Note that all FPs used were monomeric variants. (D) The indicated RFP-tagged constructs were transfected into N2a cells and analyzed for solubility. Cells were lysed in detergent buffer containing 0.5% Triton X-100 and 0.5% deoxycholate, the insoluble material was sedimented for 30 min in a microcentrifuge, and the supernatant (S) and pellet (P) fractions were analyzed by immunoblotting for the GFP tag. Note that all of the constructs are predominantly in the insoluble fraction, except for RFP, which was quantitatively soluble. Identical results were obtained in HeLa cells, and with different FP tags. (E) Visualization of aggregates formed by the GFP-PrP fusions (various representative constructs and images from HeLa cells are shown).

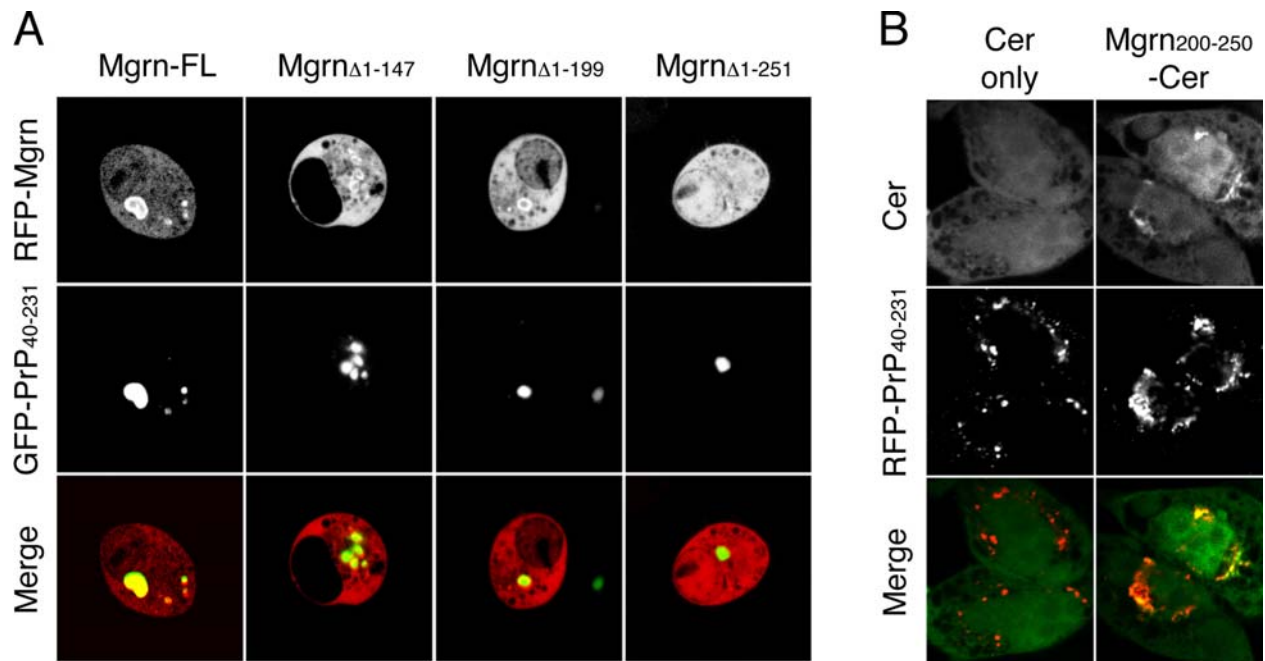


**Fig. S4. Mapping the PrP-interacting domain of Mgrn.** (A) The indicated RFP-tagged Mgrn constructs were co-transfected with GFP-PrP<sub>40-231</sub>. Representative images of co-transfected cells are shown. Note the partial co-aggregation of Mgrn around the PrP aggregate in each case except the Mgrn( $\Delta$ 1-251) construct. (B) RFP-PrP<sub>40-231</sub> was cotransfected with either Cer or Mgrn<sub>200-250</sub>-Cer (in which a 50-residue domain from Mgrn is appended to the N-terminus of Cerulean). Note that Mgrn<sub>200-250</sub>-Cer partially co-aggregates with RFP-PrP<sub>40-231</sub>, while Cer alone does not.

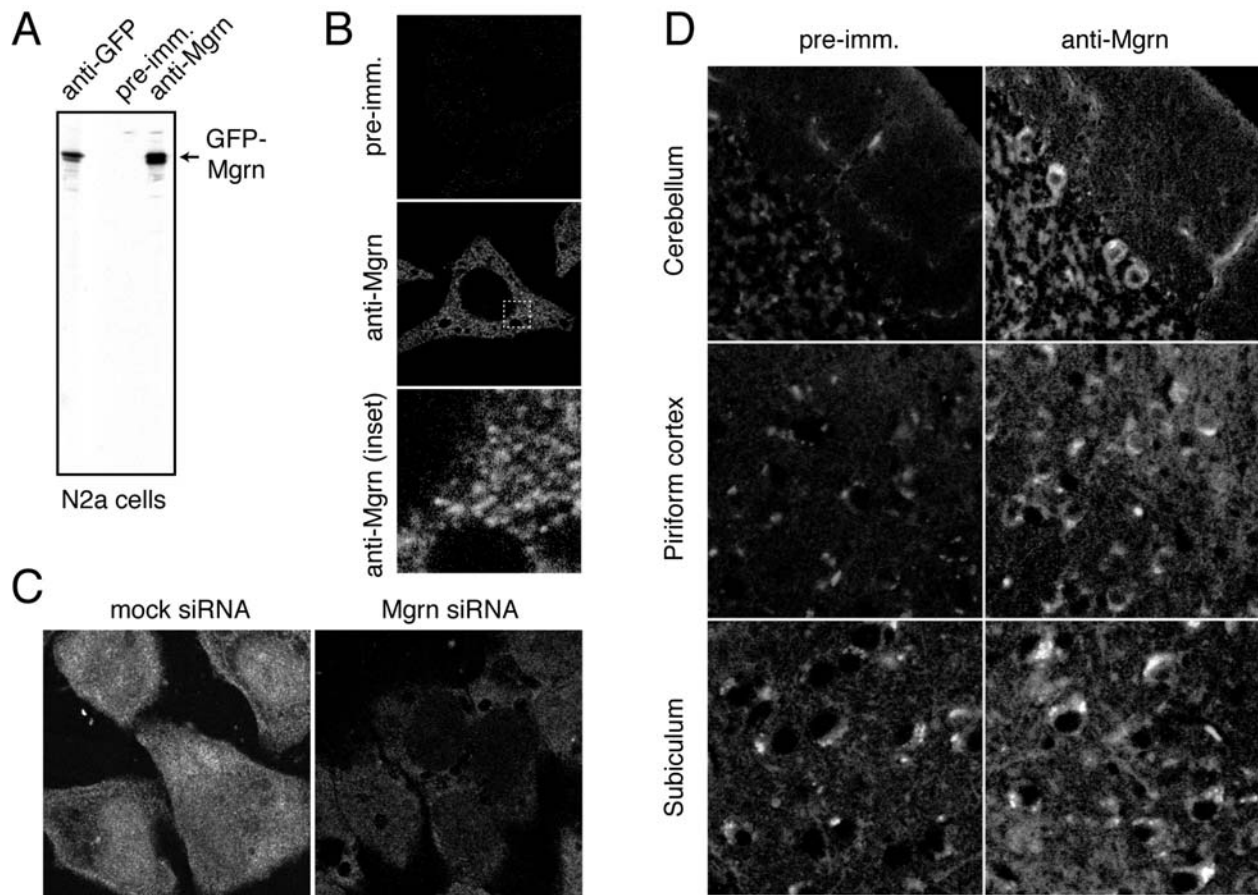


**Fig. S5. Characterization of anti-Mgrn antibody.** (A) N2a cells (which do not express any Mgrn) were transfected with GFP-Mgrn and the total cell lysate immunoblotted with anti-GFP, pre-immune serum, and anti-Mgrn. (B) HeLa cells were immunostained with either pre-immune serum or anti-Mgrn as indicated. An enlargement showing the typical punctate/vesicular pattern is also shown. (C) HeLa cells were treated with either control or Mgrn siRNAs and immunostained for Mgrn 48 hours later. The two images were captured using identical microscope settings. (D) Brain sections from an adult FVB mouse were immunostained with either pre-immune serum or anti-Mgrn as indicated. Three regions of the brain are shown. Note the autofluorescence to varying degrees in different brain regions seen with the pre-immune serum. Staining cells showed diffuse signal throughout the cytoplasm, and is especially prominent in Purkinje cells of the cerebellum.

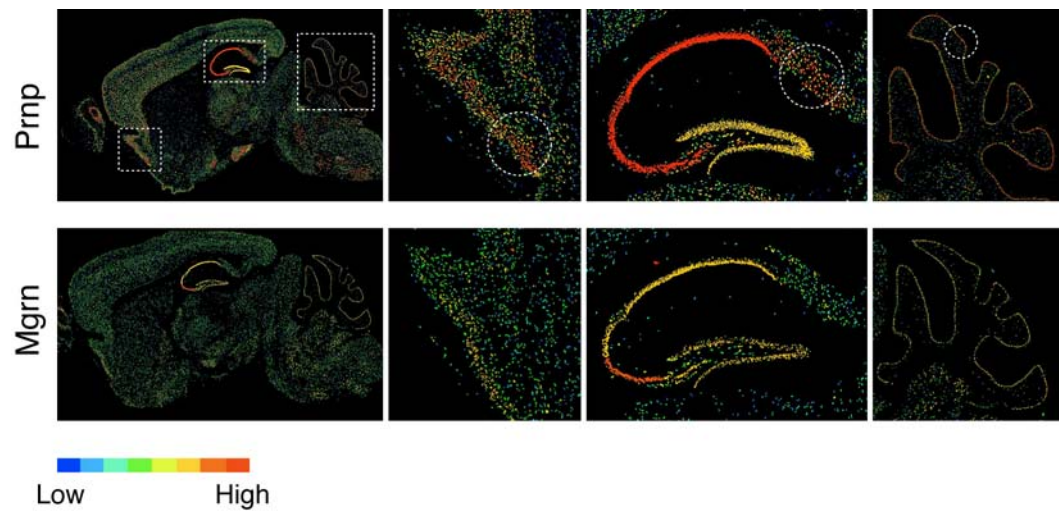


**Fig. S6. Expression patterns of Mgrn and PrP in brain.** In situ hybridization data from the Allen Brain Atlas study for PrP and Mgrn are shown, pseudo colored to indicate relative expression levels (scale below images). Enlarged views corresponding to the regions analyzed in Fig. 6 are also displayed, with the specific areas circled. These areas correspond to the piriform cortex (left), subiculum, near the hippocampus (middle), and cerebellum (right).

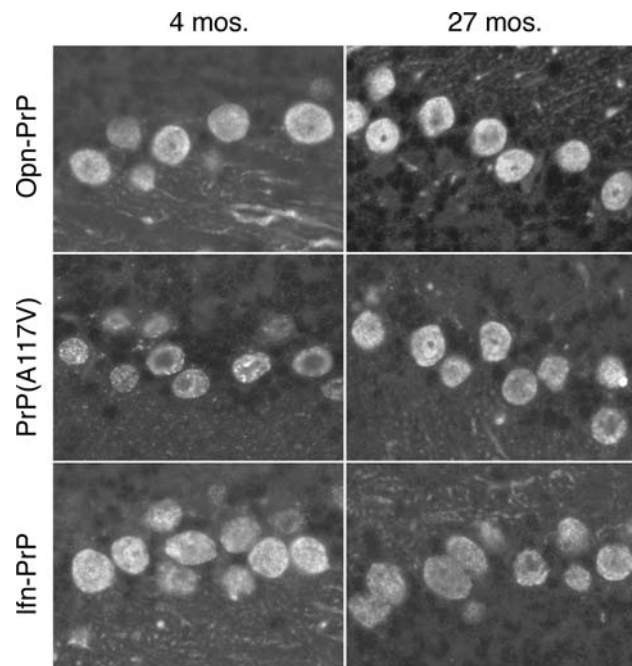


**Fig. S7. Analysis of Purkinje cells in transgenic mice.** Brain sections from the indicated transgenic mice were immunostained with anti-Calbindin to reveal Purkinje cells of the cerebellum. No loss of Purkinje cells was observed in either young or old mice.

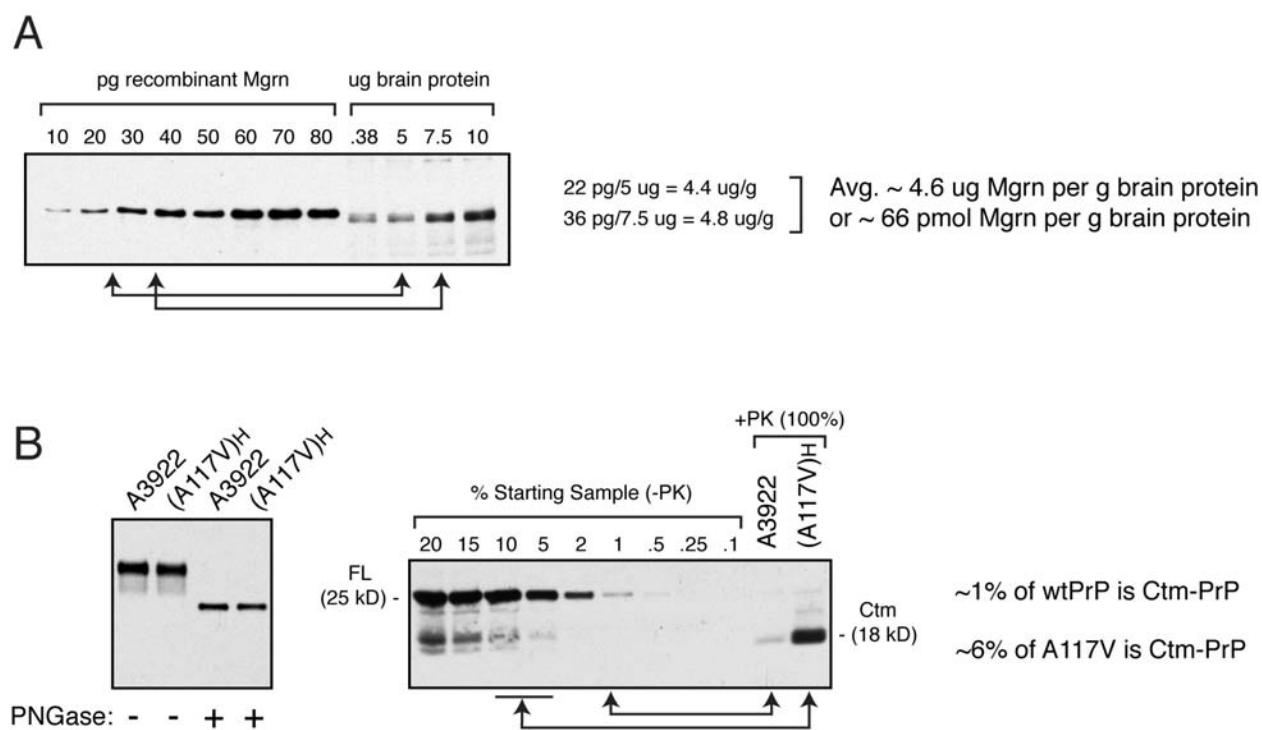


**Fig. S8. Quantification of Mgrn and <sup>Ctm</sup>PrP levels in brain.** (A) Immunoblot of defined amounts (in pg) of His-tagged recombinant Mgrn relative to the indicated amounts (in ug) of total brain protein. Quantification showed an average of ~4.6 ug Mgrn per g total brain protein. For comparison, previous quantification of PrP from multiple studies showed its abundance to be between 70 and 200 ug per g total brain protein (or ~30- to 85-fold molar excess above Mgrn). (B) The left panel shows equal amounts of brain homogenate from Tg mice expressing either wtPrP (A3922 line) or A117V (see Hegde et al., 1998) immunoblotted for PrP before and after deglycosylation with PNGase F. Note equal expression levels. The last two lanes of the right panel show the same homogenates analyzed for <sup>Ctm</sup>PrP by limited digestion with proteinase K (PK) as described in Hegde et al. (1998). In this assay, <sup>Ctm</sup>PrP generates a characteristic 18 kD product. Note that the A117V sample shows more <sup>Ctm</sup>PrP than A3922, as previously described (Hegde et al., 1998). Comparison to a dilution series of undigested A3922 brain homogenate allowed the estimation of <sup>Ctm</sup>PrP levels at 1% and 6% for wtPrP and A117V, respectively. All samples were deglycosylated with PNGase F prior to analysis. The arrows indicate the lanes that proved to be roughly equivalent upon quantification.